

Continuous-Time Control Synthesis for Multiple Quadrotors under Signal Temporal Logic Specifications

Yating Yuan*, Yu Liu*

Abstract—Continuous-time control of multiple quadrotors in constrained environments under signal temporal logic (STL) specifications is critical due to their nonlinear dynamics, safety constraints, and the requirement to ensure continuous-time satisfaction of the specifications. To ensure such control, a two-stage framework is proposed to address this challenge. First, based on geometric control, a Lyapunov-based analysis of the rotational tracking dynamics is performed to facilitate multidimensional gain design. In addition, tracking-error bounds for subsequent STL robustness analysis are derived. Second, using the tracking-error bounds, a mixed-integer convex programming (MICP)-based planning framework with a backward-recursive scheme is developed. The framework is used to generate reference trajectories that satisfy multi-agent STL tasks while meeting the trajectory requirements imposed by geometric control. Numerical simulations demonstrate that, compared with uniform gains, the optimized multidimensional gains yield less conservative time-varying bounds, mitigate oscillations, and improve transient performance, while the proposed framework ensures the satisfaction of multi-agent STL tasks in constrained environments with provable tracking guarantees.

Index Terms—Signal temporal logic planning, multiple quadrotors, geometric control

I. INTRODUCTION

As drone technology advances, quadrotors are increasingly used to execute complex tasks in confined environments, such as narrow passages and regions with tight terminal constraints [1]. To formally specify such tasks, signal temporal logic (STL) provides a language over continuous signals with explicit temporal semantics. However, guaranteeing continuous-time STL satisfaction for nonlinear systems remains an open challenge [2], especially for multi-agent systems that require both coordination and formal guarantees [3].

Various approaches have been proposed to ensure STL satisfaction in multi-agent systems. Among these, model predictive control (MPC) has been widely adopted due to its efficiency and ability to handle complex constraints and uncertainty [4]–[8]. In [4], an MPC-based controller is employed for multi-agent systems subject to continuous-time STL specifications. A stricter specification is defined by tightening temporal intervals and predicates [9]. Smooth robustness is also adopted to improve efficiency in multi-agent tasks [10], although this relaxation may compromise

soundness [11]. Another line of work applies distributed MPC (DMPC) to cooperative control in multi-agent systems by solving local problems with neighbor communication, thereby offering a balance between scalability and coordination [5]–[8]. While effective in improving efficiency in multi-agent systems, these methods generally lack formal guarantees of continuous-time STL satisfaction. In particular, existing efforts address this challenge by assuming piecewise-constant inputs and exploiting the Lipschitz continuity of robustness functions to extend discrete-time results to continuous time [8]. However, the guarantees obtained under these assumptions remain conditional and conservative, and the iterative nature of DMPC introduces additional computational cost.

Alternatively, closed-loop strategies such as control barrier functions (CBFs) and prescribed performance control (PPC) directly enforce continuous-time STL satisfaction through real-time state-feedback control. Decentralized time-varying CBFs with switching logic are proposed in [12]. However, guarantees of fixed-time constraint satisfaction are not provided, since the time required for constraint satisfaction is not uniformly bounded over the set of initial conditions. Fixed-time CBFs (TFCBFs) with least-violation optimization are introduced in [13] to handle task conflicts. Higher-order CBFs combined with feedback linearization are employed in [14] for temporal waypoint tracking. PPC provides guarantees for prescribed transient and steady-state performance [15], and it has also been extended to multi-agent systems under STL tasks. Formation and sequencing tasks are addressed in [16], leader-follower coordination is considered in [17], and a contract-based decomposition for distributed implementation is introduced in [18]. While these methods enable feedback-based task enforcement in continuous time, they remain limited to specific specifications, require careful parameter tuning, and may suffer from input discontinuities under switching.

Additionally, nonlinear feedback controllers with bounded tracking-error guarantees have been integrated with STL planning methods to ensure continuous-time satisfaction in [19] and [20]. However, such approaches tend to be conservative in narrow environments due to the use of uniform tracking-error bounds. Moreover, for quadrotor applications, conventional controllers formulated in Euclidean coordinates, such as decoupled position-attitude controllers based on Euler angles, may suffer from coordinate singularities and inconsistent position-attitude coordination. In this context, geometric control on $SE(3)$ [21]–[26] avoids coordinate singularities, thereby enabling agile maneuvers and direct

Yating Yuan is with the Department of Applied Mathematics, University of Waterloo, 200 University Avenue, Waterloo, Ontario, Canada N2L3G1. Yu Liu is with the College of Urban Transportation and Logistics, Shenzhen Technology University, 3002 Lantian Road, Shenzhen, Guangdong, China, 518118. *The corresponding authors. (email: yating.yuan@uwaterloo.ca; liuyu@sztu.edu.cn).

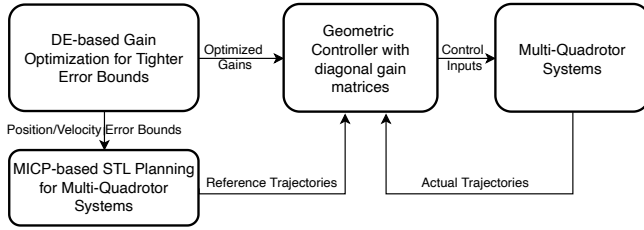


Fig. 1: Configuration of the proposed framework with continuous-time STL robustness guarantees.

handling of quadrotor dynamics.

In this work, we propose a control-synthesis framework based on geometric control, as illustrated in Fig. 1. Differential evolution (DE) is employed to tune the diagonal gain matrices, yielding time-varying bounds on the position and velocity errors. These bounds are then incorporated into the MIPC-based STL planner to generate reference trajectories such that the actual trajectories satisfy the STL specifications. The main contributions of this paper are summarized as follows: 1) A geometric controller with multidimensional gains is developed by generalizing the scalar gains in [26] to diagonal positive-definite gain matrices. Based on a Lyapunov analysis of the tracking errors and a differential-evolution-based procedure for gain selection, the proposed method yields less conservative error bounds that decay exponentially. Numerical simulations further demonstrate faster convergence, reduced oscillations, and improved transient performance. 2) The continuous-time STL framework with Bézier curves proposed in [27] is extended to multi-agent systems by incorporating a backward-recursive structure [28] into the MIPC encoding, thereby improving computational efficiency. Both the reference and tracked trajectories satisfy the same multi-agent continuous-time STL specifications, while the reference trajectories additionally satisfy the requirements imposed by the geometric controller.

The rest of the paper is organized as follows. Section II introduces the preliminaries on quadrotor dynamics, geometric control, Bézier curves, and STL. Section III formulates the control-synthesis problem under STL specifications. Section IV analyzes the error bounds under the initial conditions and presents a differential-evolution-based optimization for gain selection. Section V presents the MIPC-based optimization problem for generating reference trajectories for multiple quadrotors. Simulation results and illustrative examples are provided in Section VI, and Section VII concludes the paper.

II. PRELIMINARIES

Notation: Let $\mathbb{Y} \subset \mathbb{R}^3$ denote the workspace. Let $\mathbf{1}_d \in \mathbb{R}^d$ denote the all-ones vector, and let $Id, 0d \in \mathbb{R}^{d \times d}$ denote the identity and zero matrices, respectively. Let $\mathbb{R}_{++}^d := \{x \in \mathbb{R}^d \mid x_i > 0, \forall i = 1, \dots, d\}$ be the set of strictly positive d -dimensional real vectors. For brevity, $\mathbb{R}_{++} := \mathbb{R}_{++}^1$ denotes the set of strictly positive real numbers, and \mathbb{S}_{++}^n denotes the set of $n \times n$ symmetric positive-definite matrices. For any $a \in \mathbb{R}^d$, $|a|$ denotes the element-wise absolute value, and $\|a\|$ is the Euclidean norm. The maximum and

TABLE I: Physical variables in quadrotor dynamics.

Symbol	Physical meaning
\mathcal{I}	Inertial frame $\mathcal{I} = \{e_1, e_2, e_3\}$
$\mathcal{B}(t)$	Body frame $\mathcal{B}(t) = \{b_1(t), b_2(t), b_3(t)\}$
$m \in \mathbb{R}$	Total mass
$g \in \mathbb{R}$	Gravitational acceleration $g = 9.81 \text{ m/s}^2$
$J \in \mathbb{S}_{++}^3$	Positive-definite inertia matrix
$p(t) \in \mathbb{R}^3$	Position of the center of mass
$v(t) \in \mathbb{R}^3$	Velocity of the center of mass
$R(t) \in \text{SO}(3)$	Rotation matrix with $b_i(t) = R(t)e_i, i \in \{1, 2, 3\}$
$\omega(t) \in \mathbb{R}^3$	Angular velocity in the body-fixed frame
$f_i(t) \in \mathbb{R}$	Thrust of the i -th propeller along $b_3(t)$
$f(t) \in \mathbb{R}$	Total thrust $f(t) = \sum_{i=1}^4 f_i(t)$
$\tau(t) \in \mathbb{R}^3$	Torque

minimum eigenvalues of a matrix A are denoted by $\bar{\lambda}(A)$ and $\underline{\lambda}(A)$, and $\text{tr}(A)$ denotes its trace. Let $T > 0$ define the time horizon, and $\mathbb{T} = [0, T]$. For a signal $y : \mathbb{T} \rightarrow \mathbb{Y}$, its portion to an interval $[t_i, t_j]$ is defined as $(y, [t_i, t_j]) := \{y(t) \mid t \in [t_i, t_j]\}$. For brevity, the suffix of the signal y starting at time t is denoted by $(y, t) := (y, [t, T])$. Define a convex polytope $\text{Poly}(H, b) := \{x \in \mathbb{R}^d \mid Hx \leq b\}$, with $H \in \mathbb{R}^{r \times d}$ and $b \in \mathbb{R}^r$. Let H_i and b_i denote the i -th row of H and entry of b , respectively. The number of rows in H is denoted $\text{Row}(H)$.

A. Quadrotor Dynamics Model

Table I lists the physical variables of the quadrotor dynamics model. As depicted in Fig. 2, let $\mathcal{I} = e_1, e_2, e_3$ denote an inertial frame, where e_1 and e_2 span the horizontal plane and e_3 points upward, opposite to the direction of gravity. Let $\mathcal{B}(t) = \{b_1(t), b_2(t), b_3(t)\}$ be the body-fixed frame attached to the quadrotor center of mass, where $b_1(t)$, $b_2(t)$, and $b_3(t)$ denote the forward, lateral, and thrust directions, respectively.

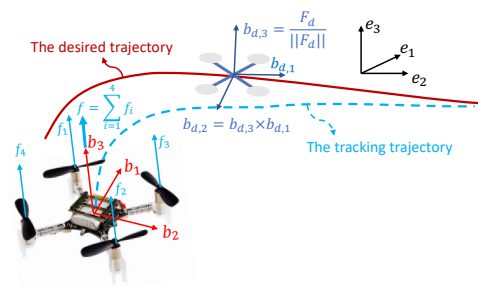


Fig. 2: The inertial frame \mathcal{I} , the body frame \mathcal{B} , and desired body axes $b_{d,1}(t)$, $b_{d,2}(t)$, $b_{d,3}(t)$ representing the desired orientation $R_d(t)$.

The configuration space of the quadrotor is the special Euclidean group $\text{SE}(3)$, parameterized by a position $p \in \mathbb{R}^3$ and a rotation matrix $R \in \text{SO}(3)$. The Lie algebra $\mathfrak{so}(3)$ of $\text{SO}(3)$ is the space of skew-symmetric matrices. The hat map $\wedge : \mathbb{R}^3 \rightarrow \mathfrak{so}(3)$ is defined by $x \mapsto \hat{x}$, where $\hat{x}y = x \times y$ for all $y \in \mathbb{R}^3$. The vee map $(\cdot)^\vee : \mathfrak{so}(3) \rightarrow \mathbb{R}^3$ denotes the inverse of \wedge [29, Chapter 3].

The quadrotor dynamics are given by [22]:

$$\dot{p}(t) = v(t), \quad (1)$$

$$\dot{v}(t) = -ge_3 + m^{-1}f(t)R(t)e_3, \quad (2)$$

$$\dot{R}(t) = R(t)\hat{\omega}(t), \quad (3)$$

$$\dot{\omega}(t) = J^{-1}(-\omega(t) \times J\omega(t) + \tau(t)), \quad (4)$$

B. Geometric Control

Let $y_d : \mathbb{T} \rightarrow \mathbb{Y}$ be a desired \mathcal{C}^4 position trajectory¹. As presented in Fig. 2, the desired rotation matrix $R_d(t) = [b_{d,1}(t), b_{d,2}(t), b_{d,3}(t)] \in \text{SO}(3)$ where $b_{d,1}(t)$, $b_{d,2}(t)$ and $b_{d,3}(t)$ are chosen as follows [22]. The corresponding angular velocity is $\omega_d(t) = (R_d^\top(t)\dot{R}_d(t))^\vee \in \mathbb{R}^3$. Moreover, an assumption is imposed on the desired acceleration for the subsequent error-bound analysis.

Assumption 1 ([26]): Assume that there exists a positive vector $b_a \in \mathbb{R}_{>0}^3$ such that the second-order derivative of y_d satisfies the following element-wise absolute value inequality:

$$|mge_3 + m\ddot{y}_d(t)| \leq b_a, \forall t \in \mathbb{T} \quad (5)$$

Let $y_{tr} : \mathbb{T} \rightarrow \mathbb{R}^3$ be a tracking trajectory with rotation matrix $R(t) \in \text{SO}(3)$ and angular velocity $\omega(t) \in \mathbb{R}^3$. The positive gain matrices K_p , K_v , K_R , and $K_\omega \in \mathbb{S}_{++}^3$ are defined as $K_* = \text{diag}(k_{*1}, k_{*2}, k_{*3})$, for $*$ in $\{p, v, R, \omega\}$. Define the position error, velocity error, weighted rotational error, and angular velocity error by $e_p(t)$, $e_v(t)$, $e_{K,R}(t)$, and $e_\omega(t) \in \mathbb{R}^3$, respectively, and define the attitude error function by $\Psi_K(t) \in \mathbb{R}$ [24]:

$$e_p(t) := y_{tr}(t) - y_d(t), \quad (6)$$

$$e_v(t) := \dot{y}_{tr}(t) - \dot{y}_d(t), \quad (7)$$

$$e_{K,R}(t) := \frac{1}{2} (K_R R_d^\top(t) R(t) - R^\top(t) R_d(t) K_R)^\vee, \quad (8)$$

$$e_\omega(t) := \omega(t) - R^\top(t) R_d(t) \omega_d(t), \quad (9)$$

$$\Psi_K(t) := \frac{1}{2} \text{tr} (K_R (\mathbf{I}_3 - R_d^\top(t) R(t))). \quad (10)$$

This assumption bounds the reference trajectory's acceleration and facilitates subsequent analysis of the error bounds.

Proposition 1 ([24, Prop. 1]): Supposing K_R has distinct positive diagonal entries, define

$$h_1 = \min \{k_{R_1} + k_{R_2}, k_{R_1} + k_{R_3}, k_{R_2} + k_{R_3}\},$$

$$h_2 = \max \left\{ (k_{R_1} - k_{R_2})^2, (k_{R_1} - k_{R_3})^2, (k_{R_2} - k_{R_3})^2 \right\},$$

$$h_3 = \max \{k_{R_1} + k_{R_2}, k_{R_1} + k_{R_3}, k_{R_2} + k_{R_3}\}.$$

If $\Psi_K(t) < \psi < h_1$ for some positive ψ , then

$$g_1 \|e_{K,R}(t)\|^2 \leq \Psi_K(t) \leq g_2 \|e_{K,R}(t)\|^2, \quad (11)$$

where $g_1 = \frac{h_1}{h_2 + h_3^2}$ and $g_2 = \frac{h_3}{h_1(h_1 - \psi)}$.

¹A curve is \mathcal{C}^k if it is k -times continuously differentiable. Note the fourth derivative of the reference trajectory is required to compute the derivative of angle velocity.

C. Bézier Curves

In this work, the reference trajectory $y_d(t)$ is parameterized by an N -segment Bézier spline with a uniform time interval $\Delta t = \frac{T}{N}$:

$$y_d(t) = B_k(t), \quad t \in [t_k, t_{k+1}], \quad (12)$$

where $t_k = k\Delta t$ for $k = \{0, 1, \dots, N-1\}$. Each $B_k(t)$ is an n -degree Bézier curve defined as

$$B_k(t) = \sum_{i=0}^n b_i^n(\tau) c_{k,i}, \quad \tau = \frac{t - t_k}{\Delta t} \in [0, 1], \quad (13)$$

where $c_{k,i}$ is the i -th control point of the k -th Bézier curve and $b_i^n(\tau)$ is the i -th Bernstein polynomial of degree n . Since $\sum_{i=0}^n b_i^n(\tau) = 1$ for any $\tau \in [0, 1]$, this implies that each $B_k(t)$ lies within the convex hull $\text{conv}\{c_{k,0}, \dots, c_{k,n}\} = \{\sum_{i=0}^n \lambda_i c_{k,i} \mid \lambda_i \geq 0, \sum_{i=0}^n \lambda_i = 1\}$.

D. Signal Temporal Logic

Let $x \in \mathbb{R}^3$ and let $\mu : \mathbb{R}^3 \rightarrow \mathbb{R}$ be a predicate function. An atomic predicate is defined as $\pi := \mu(x) \geq 0$. Throughout this paper, STL formulas are considered in positive normal form (PNF) [30]. The syntax of STL is defined as:

$$\varphi := \pi \mid \neg\varphi \mid \varphi_1 \wedge \varphi_2 \mid \varphi_1 \vee \varphi_2 \mid \varphi_1 \mathcal{U}_I \varphi_2, \quad (14)$$

where \neg , \wedge , \vee , and \mathcal{U} are negation, conjunction, disjunction, and until operators, respectively, and $I = [a, b] \subseteq \mathbb{T}$ is a bounded time interval with $a < b$. The temporal operators *Eventually* (\diamond) and *Always* (\square) can be formulated by the above operators, $\diamond_I \varphi := \text{True} \mathcal{U}_I \varphi$ and $\square_I \varphi := \neg(\diamond_I \neg\varphi)$.

Definition 1: (STL semantics [31]) Given an STL specification φ and a continuous-time signal $y : \mathbb{T} \rightarrow \mathbb{Y}$, the semantics of STL are defined over the suffixes (y, t) as

$$\begin{aligned} (y, t) \models \pi &\Leftrightarrow \mu(y(t)) \geq 0; \\ (y, t) \models \neg\varphi &\Leftrightarrow \neg((y, t) \models \varphi); \\ (y, t) \models \varphi_1 \wedge \varphi_2 &\Leftrightarrow (y, t) \models \varphi_1 \wedge (y, t) \models \varphi_2; \\ (y, t) \models \varphi_1 \vee \varphi_2 &\Leftrightarrow (y, t) \models \varphi_1 \vee (y, t) \models \varphi_2; \\ (y, t) \models \diamond_I \varphi &\Leftrightarrow \exists t' \in \tilde{I}, (y, t') \models \varphi; \\ (y, t) \models \square_I \varphi &\Leftrightarrow \forall t' \in \tilde{I}, (y, t') \models \varphi; \\ (y, t) \models \varphi_1 \mathcal{U}_I \varphi_2 &\Leftrightarrow \exists t' \in \tilde{I} (y, t') \models \varphi_2 \\ &\quad \wedge \forall t'' \in [t, t'], (y, t'') \models \varphi_1, \end{aligned}$$

where $\tilde{I} = (t + I) \cap \mathbb{T}$ and $t + I = [t + a, t + b]$. The notation $(y, t) \models \varphi$ denotes that the signal suffix (y, t) satisfies the STL formula φ , whereas $(y, t) \not\models \varphi$ denotes that it does not. For brevity, write $y \models \varphi$ when $(y, 0) \models \varphi$.

To characterize STL satisfaction of each agent's trajectory, the notion of a time-varying robust trajectory in [32] is extended to multi-agent systems, as formalized in Definition 2.

Definition 2 (Agent-wise time-varying robust trajectory): Given an STL specification φ and a function $\rho^{\ell, \varphi} : \mathbb{T} \rightarrow \mathbb{R}_+$ for any agent $\ell \in \{1, \dots, L\}$, the trajectory $y^\ell : \mathbb{T} \rightarrow \mathbb{Y}$ is said to be time-varying robust if $y^\ell \models \varphi$, and any trajectory $\tilde{y}^\ell : \mathbb{T} \rightarrow \mathbb{Y}$ satisfying

$$\|\tilde{y}^\ell(t) - y^\ell(t)\| \leq \rho^{\ell, \varphi}(t), \quad \forall t \in \mathbb{T}, \quad (15)$$

also satisfies φ .

III. PROBLEM STATEMENT

Given an STL specification φ , the objective is to synthesize reference trajectories and a feedback controller for multiple quadrotors such that the actual tracking trajectory y_{tr}^ℓ of each quadrotor ℓ satisfies φ . To formalize the required robustness margin, define the lower bound on the time-varying robustness as

$$\gamma(t) := \Gamma(t) + \gamma_c, \quad t \in \mathbb{T}. \quad (16)$$

where $\gamma_c > 0$ is a constant safety margin and $\Gamma : \mathbb{T} \rightarrow \mathbb{R}_{>0}$ is a non-increasing function. In this work, $\Gamma(t)$ characterizes a time-varying bound on the position tracking error, and γ_c serves as a physical safety margin such as the quadrotor size.

Thus, if for each agent ℓ and all $t \in \mathbb{T}$, the reference trajectory y_d^ℓ satisfies φ with robustness margin $\rho^{\ell,\varphi}(t)$ and $\rho^{\ell,\varphi}(t) \geq \gamma(t) > \Gamma(t)$, then

$$\|y_{tr}^\ell(t) - y_d^\ell(t)\| \leq \Gamma(t) < \rho^{\ell,\varphi}(t) \Rightarrow y_{tr}^\ell \models \varphi. \quad (17)$$

This overall objective can be divided into the following two sub-objectives:

Objective 1: Optimize the multidimensional control gains for the geometric controller to obtain a non-increasing time-varying bound $\Gamma(t)$ on the tracking error.

Objective 2: Given an STL specification φ , generate a reference trajectory y_d^ℓ in (12) for each agent ℓ , such that $y_d^\ell \models \varphi$ with robustness margin $\rho^{\ell,\varphi}(t) \geq \gamma(t) > \Gamma(t)$, while ensuring multi-agent safety, smoothness, and compliance with the kinematic requirements imposed by the geometric controller.

IV. TRACKING ERROR BOUNDS

In this section, the tracking error bounds induced by the geometric controller are analyzed in Section IV-A. An optimization problem is formulated in Section IV-B to select the multidimensional control gains for $\Gamma(t)$ in *Objective 1*.

With multidimensional gains, the control force $f(t)$ and torque $\tau(t)$ are defined as

$$f(t) = F_d^\top(t)R(t)e_3, \quad (18)$$

$$F_d(t) = -K_p e_p(t) - K_v e_v(t) + mge_3 + m\ddot{y}_d(t), \quad (19)$$

$$\begin{aligned} \tau(t) = & -e_{K,R}(t) - K_\omega e_\omega(t) + \omega(t) \times J\omega(t) \\ & - J(\dot{\omega}(t)R^\top(t)R_d(t)\omega_d(t) - R^\top(t)R_d(t)\dot{\omega}_d(t)). \end{aligned} \quad (20)$$

Here, for all $t \in \mathbb{T}$, it is assumed that $\|F_d(t)\| \neq 0$ and $F_{d,3}(t) \neq -\|F_d(t)\|$, so that the desired rotation matrix $R_d(t)$ is well defined. Similar assumptions have been adopted in related studies such as [22] and [26].

A. Time-varying Error Bounds Analysis

Tracking error bounds are derived through Lyapunov analysis of the translational and rotational tracking errors.

1) Lyapunov Function for Translation Error: Let $z_1^\top(t) := [e_p^\top(t) \quad e_v^\top(t)]$ be the translation-error vector, and let the translation Lyapunov candidate function \mathcal{V}_1 be

$$\mathcal{V}_1(t) := z_1^\top(t)M_1z_1(t), \quad (21)$$

where $\nu_1 \in (0, 1)$ is a tuning constant and

$$M_1 = \frac{1}{2} \begin{bmatrix} K_p & c_1 I_3 \\ c_1 I_3 & m I_3 \end{bmatrix} \in \mathbb{S}_{++}^6, \quad (22)$$

$$c_1 = \nu_1 \min \left\{ \sqrt{m\lambda(K_p)}, \min_{i=1,2,3} \left(\frac{4mk_{p_i}k_{v_i}}{k_{v_i}^2 + 4mk_{p_i}} \right) \right\}. \quad (23)$$

Then, the time derivative of $\mathcal{V}_1(t)$ is

$$\dot{\mathcal{V}}_1(t) = -z_1^\top(t)W_1z_1(t) - \Delta_f^\top(t) \begin{bmatrix} c_1 I_3 \\ I_3 \end{bmatrix} z_1(t), \quad (24)$$

where

$$W_1 = \frac{1}{2m} \begin{bmatrix} 2c_1K_p & c_1K_v \\ c_1K_v & 2m(K_v - c_1I_3) \end{bmatrix} \in \mathbb{S}_{++}^6, \quad (25)$$

$$\Delta_f(t) = \|F_d(t)\| \left((b_{3,d}^\top(t)b_3(t))b_3(t) - b_{3,d}(t) \right) \quad (26)$$

2) Lyapunov Function for Rotational Error: Let $z_2^\top(t) := [e_{K,R}^\top(t) \quad e_\omega^\top(t)]$ be the rotational-error vector, and let the rotational Lyapunov candidate function be

$$\mathcal{V}_2(t) := \frac{1}{2} e_\omega^\top(t)J e_\omega(t) + \Psi_K(t) + c_2 e_{K,R}^\top(t) e_\omega(t), \quad (27)$$

where

$$c_2 := \nu_2 \min \left\{ \sqrt{2g_m\lambda(J)}, \frac{\sqrt{2\lambda(K_\omega)}}{\text{tr}(K_R)}, \min_{i=1,2,3} \frac{4J_i k_{\omega_i}}{2\sqrt{2}J_i \text{tr}(K_R) + k_{\omega_i}^2} \right\}, \quad (28)$$

with a tuning constant $\nu_2 \in (0, 1)$ and $g_m = \min\{g_1, g_2\}$. Here, g_1 and g_2 are as defined in Proposition 1. From (11), $\mathcal{V}_2(t)$ is bounded by

$$z_2^\top(t)M_{2,1}z_2(t) \leq \mathcal{V}_2(t) \leq z_2^\top(t)M_{2,2}z_2(t), \quad (29)$$

where $M_{2,1}, M_{2,2} \in \mathbb{S}_{++}^6$ are defined as

$$M_{2,1} = \frac{1}{2} \begin{bmatrix} 2g_1 I_3 & c_2 I_3 \\ c_2 I_3 & J \end{bmatrix}, M_{2,2} = \frac{1}{2} \begin{bmatrix} 2g_2 I_3 & c_2 I_3 \\ c_2 I_3 & J \end{bmatrix}. \quad (30)$$

The time derivative $\dot{\mathcal{V}}_2(t)$ satisfies:

$$\dot{\mathcal{V}}_2(t) \leq -z_2^\top(t)W_2z_2(t), \quad (31)$$

where

$$W_2 = \begin{bmatrix} c_2 J^{-1} & \frac{c_2}{2} K_\omega J^{-1} \\ \frac{c_2}{2} K_\omega J^{-1} & K_\omega - \frac{c_2}{\sqrt{2}} \text{tr}(K_R) I_3 \end{bmatrix} \in \mathbb{S}_{++}^6. \quad (32)$$

3) *Time-varying Lyapunov Function Bounds*: (See I for details.)

From (29) and (31), together with the Rayleigh quotient inequality [33, Section 4.2], it follows that

$$\dot{\mathcal{V}}_2(t) \leq -\lambda \left(M_{2,2}^{-\frac{1}{2}} W_2 M_{2,2}^{-\frac{1}{2}} \right) \mathcal{V}_2(t). \quad (33)$$

Applying the comparison principle in [34, Section 3.4] yields

$$\mathcal{V}_2(t) \leq e^{-\beta t} \mathcal{V}_2(0), \quad \beta := \lambda \left(M_{2,2}^{-\frac{1}{2}} W_2 M_{2,2}^{-\frac{1}{2}} \right). \quad (34)$$

Define the bound $\mathcal{L}_2(\mathcal{V}_2(0), t) := e^{-\frac{\beta}{2}t} \sqrt{\mathcal{V}_2(0)}$, then,

$$\sqrt{\mathcal{V}_2(t)} \leq \mathcal{L}_2(\mathcal{V}_2(0), t). \quad (35)$$

Moreover, using the bound on $\Psi_K(t)$ in (11) and Rodrigues' formula [35, Lemma 2.3], one obtains an upper bound on $\|\Delta_f(t)\|$. Consequently, (24) yields

$$\dot{\mathcal{V}}_1(t) \leq -(\alpha_0 - \alpha_1 \sqrt{\mathcal{V}_2(t)}) \mathcal{V}_1(t) + \alpha_2 \sqrt{\mathcal{V}_2(t)} \mathcal{V}_1(t), \quad (36)$$

where

$$\alpha_0 = \lambda \left(M_1^{-\frac{1}{2}} W_1 M_1^{-\frac{1}{2}} \right), \quad (37)$$

$$\alpha_1 = \left\| [K_p, K_v] M_1^{-\frac{1}{2}} \right\|, \quad (38)$$

$$\alpha_2 = m \|b_a\| \beta', \quad (39)$$

$$\beta' = \left\| \left[\frac{c_1}{m} \mathbf{I}_3, \mathbf{I}_3 \right] M_1^{-\frac{1}{2}} \right\| \left\| [\mathbf{I}_3, 0_{3 \times 3}] M_{2,1}^{-\frac{1}{2}} \right\| \sqrt{\frac{4g_2}{h_1}}. \quad (40)$$

Since $\sqrt{\mathcal{V}_2(t)} \leq \mathcal{L}_2(\mathcal{V}_2(0), t)$, applying the comparison principle in [34, Section 3.4] to (36) together with (35) yields $\sqrt{\mathcal{V}_1(t)} \leq \mathcal{L}_1(\mathcal{V}_1(0), \mathcal{V}_2(0), t)$, where

$$\mathcal{L}_1(\mathcal{V}_1(0), \mathcal{V}_2(0), t) = e^{-\frac{\alpha_0 t}{2}} \left[e^{\frac{\alpha_1 \sqrt{\mathcal{V}_2(0)}}{\beta}} \sqrt{\mathcal{V}_1(0)} + \frac{\alpha_2 \sqrt{\mathcal{V}_2(0)}}{2} \int_0^t e^{\frac{1}{2}(\alpha_0 - \beta)s} ds \right]. \quad (41)$$

Both $\mathcal{L}_1(\mathcal{V}_1(0), \mathcal{V}_2(0), t)$ and $\mathcal{L}_2(\mathcal{V}_2(0), t)$ decay exponentially with time, depending on the initial values $\mathcal{V}_1(0)$ and $\mathcal{V}_2(0)$.

Proposition 2 (Initial conditions (See II)): Let $y_d : \mathbb{T} \rightarrow \mathbb{R}^3$ be a \mathcal{C}^4 trajectory satisfying (5). Define $\psi := \lambda(K_R) \psi_K$ and $\psi_K \in \left(0, \frac{h_1}{\lambda(K_R)}\right)$, so that $\psi \in (0, h_1)$. Assume that, for some $\alpha_\psi \in [0.5, 1)$ and $\bar{\mathcal{V}}_1 > 0$, the initial conditions satisfy

$$\Psi_K(0) < \alpha_\psi \psi, \quad (42)$$

$$\frac{1}{2} e_\omega^\top(0) J e_\omega(0) \leq (1 - \alpha_\psi) \psi, \quad (43)$$

$$\mathcal{V}_1(0) \leq \bar{\mathcal{V}}_1. \quad (44)$$

Then, $\Psi_K(t) < \psi$ for all $t \in \mathbb{T}$, and hence the assumptions of Proposition 1 hold. Moreover, it follows that

$$\mathcal{V}_2(0) \leq \bar{\mathcal{V}}_2 := \left(1 + c_2 \sqrt{\frac{2\alpha_\psi(1 - \alpha_\psi)}{\lambda(J) g_1}} \right) \psi. \quad (45)$$

With (44) and (45), $\mathcal{L}_1(\bar{\mathcal{V}}_1, \bar{\mathcal{V}}_2, t) \geq \mathcal{L}_1(\mathcal{V}_1(0), \mathcal{V}_2(0), t)$ holds. From (21), there exist the time-varying tracking error bounds $\|e_p(t)\| \leq \mathcal{L}_p(t)$ and $\|e_v(t)\| \leq \mathcal{L}_v(t)$ where

$$\mathcal{L}_p(t) := \left\| [\mathbf{I}_3, 0_{3 \times 3}] M_1^{-\frac{1}{2}} \right\| \mathcal{L}_1(\bar{\mathcal{V}}_1, \bar{\mathcal{V}}_2, t), \quad (46)$$

$$\mathcal{L}_v(t) := \left\| [0_{3 \times 3}, \mathbf{I}_3] M_1^{-\frac{1}{2}} \right\| \mathcal{L}_1(\bar{\mathcal{V}}_1, \bar{\mathcal{V}}_2, t). \quad (47)$$

Compared with the the error bounds in [26], the proposed bounds are tighter, as they are derived directly from $\mathcal{L}_1(\bar{\mathcal{V}}_1, \bar{\mathcal{V}}_2, t)$ and thus reduce conservatism.

B. Optimization-based Control Gains

The high-dimensional nonlinear quadrotor dynamics make multidimensional control-gain selection complex, and unsuitable gains may lead to unnecessarily large upper bounds. According to (46) and (47), control gains can be chosen by minimizing the bound $\mathcal{L}_1(\bar{\mathcal{V}}_1, \bar{\mathcal{V}}_2, t)$.

Let $\zeta = \frac{\alpha_0 - \beta}{2}$. If $\zeta \neq 0$, then $\dot{\mathcal{L}}_1(\bar{\mathcal{V}}_1, \bar{\mathcal{V}}_2, t)$ is affine in $e^{\zeta t}$, and $e^{\zeta t}$ is monotone in t . If $\zeta = 0$, then $\dot{\mathcal{L}}_1(\bar{\mathcal{V}}_1, \bar{\mathcal{V}}_2, t)$ is affine in t . Therefore, the equation $\dot{\mathcal{L}}_1(\bar{\mathcal{V}}_1, \bar{\mathcal{V}}_2, t) = 0$ has at most one solution. If the equation admits a solution t_s , then it follows by direct differentiation that $\ddot{\mathcal{L}}_1(\bar{\mathcal{V}}_1, \bar{\mathcal{V}}_2, t_s) < 0$. Hence, if it exists, t_s is the unique stationary point and a local maximizer of $\mathcal{L}_1(\bar{\mathcal{V}}_1, \bar{\mathcal{V}}_2, t)$. Define $t^* := \max(0, \min(t_s, T)) \in \mathbb{T}$, with the convention that $t_s := 0$ when no solution exists. Then define

$$\mathcal{L}_{1,\max} := \max_{t \in \mathbb{T}} \mathcal{L}_1(\bar{\mathcal{V}}_1, \bar{\mathcal{V}}_2, t) = \mathcal{L}_1(\bar{\mathcal{V}}_1, \bar{\mathcal{V}}_2, t^*). \quad (48)$$

Furthermore, to satisfy the assumption in Proposition 1 that the diagonal entries of K_R are distinct, the condition $\Delta_{K_R} = \sum_{1 \leq i < j \leq 3} \Delta_{ij} = 3$ is imposed, where

$$\Delta_{ij} = \begin{cases} 1, & |K_{R_i} - K_{R_j}| \geq \epsilon_R \\ 0, & \text{otherwise.} \end{cases} \quad (49)$$

In this paper, $\epsilon_R = 1$. Problem 1 is formulated to represent *Objective 1* and can be solved by differential evolution [36], a parallelizable global optimizer for nonconvex problems that requires no initial guess.

Problem 1: The control gains $\{K_p, K_v, K_R, K_\omega\}$ and tuning parameters $\{\nu_1, \nu_2\}$ are determined by solving the following optimization problem:

$$\begin{aligned} & \arg \min_{\substack{K_p, K_v, K_R, K_\omega, \\ \nu_1, \nu_2}} \mathcal{L}_{1,\max} \\ & \text{such that } 0 < \nu_1, \nu_2 < 1, \\ & \Delta_{K_R} = 3, \\ & \underline{k} \leq K_{p_i}, K_{v_i}, K_{R_i}, K_{\omega_i} \leq \bar{k}, i \in \{1, 2, 3\}. \end{aligned} \quad (50)$$

Here, $0 < \underline{k} < \bar{k}$ are constants and denote the lower and upper bounds of the control gains, respectively.

V. REFERENCE TRAJECTORY CONSTRUCTION

Once the gains are determined by solving Problem 1, the position error bound $\mathcal{L}_p(\bar{\mathcal{V}}_1, \bar{\mathcal{V}}_2, t)$ can be obtained. Then,

according to (16), the non-increasing function $\Gamma(t)$ defining the lower bound $\gamma(t)$ is chosen $\Gamma(t) = \tilde{L}_p(t)$, where

$$\tilde{L}_p(t) = \begin{cases} \mathcal{L}_p(t^*), & \text{if } t \leq t^*, \\ \mathcal{L}_p(t), & \text{otherwise.} \end{cases} \quad (51)$$

To ensure that both the Bézier-parameterized reference trajectory and the tracking trajectory satisfy the STL specifications, *Objective 2* is formulated as Problem 2.

Problem 2: Given an STL specification φ and L quadrotors, for each quadrotor $\ell \in \{1, \dots, L\}$, as defined in (12), a desired position trajectory $y_d^\ell : \mathbb{T} \rightarrow \mathbb{R}^3$ is parameterized by N piecewise Bézier curves of degree n in (13). For any $t \in [t_k, t_{k+1}]$ and $k \in \{0, \dots, N-1\}$, the segment $B_k^\ell(t)$ has the piecewise time-varying robustness measure $\rho_k^{\ell, \varphi}(t) = \rho_k^{\ell, \varphi}(\mathcal{C}_k^\ell, a_k^\ell) \geq \gamma(t_k) = \Gamma(t_k) + \gamma_c > 0$. Here, $\rho_k^{\ell, \varphi}(\mathcal{C}_k^\ell, a_k^\ell)$ depends on the maximum acceleration $a_k^\ell \in \mathbb{R}^3$ and the control points $\mathcal{C}_k^\ell := \{c_{k,i}^\ell\}_{i=0}^n$. Let $v_k^\ell \in \mathbb{R}^3$ be the maximum velocity of B_k^ℓ . The MICP is formulated to maximize the robustness measure while minimizing the motion effort of the reference trajectory as follows:

$$\begin{aligned} \arg \min_{\substack{\mathcal{C}_k^\ell, v_k^\ell, a_k^\ell \\ l=1, k=0}} \sum_{l=1}^L \sum_{k=0}^{N-1} & -\mathcal{W} \rho_k^{\ell, \varphi}(\mathcal{C}_k^\ell, a_k^\ell) + \mathcal{Q} \|v_k^\ell\|_1 + \mathcal{R} \|a_k^\ell\|_1 \\ \text{such that } & B_k^\ell \text{ and } B_{k+1}^\ell \text{ satisfies } C^4 \text{ constraints,} \\ & B_k^\ell \text{ satisfies kinematic constraints,} \\ & \rho_k^{\ell, \varphi}(\mathcal{C}_k^\ell, a_k^\ell) \geq \gamma(t_k), \end{aligned} \quad (52)$$

where $\mathcal{W}, \mathcal{Q}, \mathcal{R} \in \mathbb{R}$ are user-defined weights. All quadrotors are assumed to share the same physical configuration and Lyapunov parameters. If different models are used, it suffices to adapt $\Gamma(t)$ for each model to account for the corresponding bounds $\gamma(t)$.

A. Continuity and Kinematic Constraints

The Bézier curves are required to satisfy the continuity and kinematic constraints, which are applied uniformly to all agents. The index ℓ is omitted in this subsection for clarity.

1) C^4 continuity constraints: To ensure C^4 continuity at the junction time $t = t_{k+1}$ between consecutive Bézier segments B_k and B_{k+1} , five constraints are imposed on their control points, expressed as follows for $q \in \{0, 1, 2, 3, 4\}$:

$$\sum_{p=0}^q (-1)^p \binom{q}{p} c_{k, n-p} = \sum_{p=0}^q (-1)^{q-p} \binom{q}{p} c_{k+1, p}. \quad (53)$$

These constraints enforce the equality between the backward finite differences of the end control points of B_k and the forward finite differences of the start control points of B_{k+1} , both evaluated at $t = t_{k+1}$.

2) *Velocity constraints:* To ensure $|\dot{y}_{\text{tr}}| \leq v_{\text{max}}$, choose $\tilde{\mathcal{L}}_v(t) = \mathcal{L}_v(t^*)$ for $t \leq t^*$ and $\tilde{\mathcal{L}}_v(t) = \mathcal{L}_v(t)$ otherwise. Let v_k be the maximum velocity of the k -th Bézier curve and impose, for all $i \in \{0, \dots, n-1\}$,

$$|c_{k, i+1} - c_{k, i}| \leq \frac{v_k \Delta t}{n}, \quad (54)$$

$$0 < v_k \leq v_{\text{max}} - \tilde{\mathcal{L}}_v(t_k) \mathbf{1}_3. \quad (55)$$

Since $\hat{B}_k(t)$ is a Bézier curve of degree $(n-1)$ and its Bernstein polynomials satisfy $\sum_{i=0}^{n-1} b_i^{n-1}(\tau) = 1$ for all $\tau \in [0, 1]$, it follows that $|\hat{B}_k(t)| \leq \frac{n}{\Delta t} \max_i |c_{k, i+1} - c_{k, i}| \leq v_k$. Therefore, by the triangle inequality, it further implies that $|\dot{y}_{\text{tr}}| \leq |\hat{B}_k(t)| + \tilde{\mathcal{L}}_v(t_k) \mathbf{1}_3 \leq v_k + \tilde{\mathcal{L}}_v(t_k) \mathbf{1}_3 \leq v_{\text{max}}$.

3) *Acceleration constraints:* Likewise, let a_k denote the maximum acceleration of the k -th Bézier curve. Define $\Delta^2 c_{k, i} := c_{k, i+2} - 2c_{k, i+1} + c_{k, i}$ for all $i \in \{0, \dots, n-2\}$. To bound the segment acceleration and enforce the condition in (5), the following acceleration constraints are imposed:

$$|\Delta^2 c_{k, i}| \leq \frac{a_k \Delta t^2}{n(n-1)}, \quad (56)$$

$$\left| g e_3 + \frac{n(n-1)}{\Delta t^2} (\Delta^2 c_{k, i})^\top e_3 \right| \leq b_a. \quad (57)$$

B. Encoding STL Satisfaction for Multi-Agent Systems

To encode the STL specification φ , a binary variable $z_k^{\ell, \varphi}$ is introduced to indicate whether the Bézier segment B_k satisfies the specification. Specifically, if z_k^{φ} is true, then $(B_k, t) \models \varphi$ for all $t \in [t_k, t_{k+1}]$.

1) *Time-varying Robustness of Bézier Curves:* The STL encoding of Bézier-curve robustness from [32] is adopted and extended to the multi-agent setting by introducing an agent index ℓ . As stated in *Problem 2*, each segment B_k^ℓ has the robustness measure $\rho_k^{\ell, \varphi}(\mathcal{C}_k^\ell, a_k^\ell) = r_k^\ell - \epsilon_k^\ell \geq \gamma(t_k)$. Here, $r_k^\ell \in \mathbb{R}_{>0}$ specifies the margin ensuring that the endpoints of the curve lie strictly within the required set, while $\epsilon_k^\ell \in \mathbb{R}_{>0}$ is the margin used to constrain the intermediate control points within the same set under acceleration constraints [32].

For completeness, the encoding in [32] is restated using the multi-agent notation adopted in this paper. Over the finite interval $\tilde{I} = (t + I) \cap \mathbb{T}$, let $k_l = k + \lfloor a/\Delta t \rfloor$ and $k_r = \min(k + 1 + \lfloor b/\Delta t \rfloor, N-1)$, and assume $k_l < k_r$.

- Predicate π :

$$z_k^{\ell, \pi} = \bigwedge_{i=1}^{\text{Row}(H)} \left(\bigwedge_{j=\{0, n\}} \frac{b_i - H_i c_{k, j}^\ell}{\|H_i\|} \geq r_k^\ell \right) \wedge z_{\epsilon_k^\ell}. \quad (58)$$

- Negation $\neg \pi$:

$$z_k^{\ell, \neg \pi} = \bigvee_{i=1}^{\text{Row}(H)} \left(\bigwedge_{j=\{0, n\}} \frac{H_i c_{k, j}^\ell - b_i}{\|H_i\|} \geq r_k^\ell \right) \wedge z_{\epsilon_k^\ell}. \quad (59)$$

where

$$\begin{aligned} z_{\epsilon_k^\ell} := & \left(\bigwedge_{j=\{1, n\}} |c_{k, j}^\ell - c_{k, j-1}^\ell| \leq \frac{a_k^\ell \Delta t^2}{2n} \right) \\ & \wedge \left(\bigwedge_{j=0}^d \frac{8\epsilon_k^\ell}{3\sqrt{d}\Delta t^2} - |a_{k, j}^\ell| \geq 0 \right). \end{aligned} \quad (60)$$

- Conjunctions $\varphi_1 \wedge \varphi_2 : z_k^{\ell, \varphi_1 \wedge \varphi_2} = z_k^{\ell, \varphi_1} \wedge z_k^{\ell, \varphi_2}$. (61)

- Disjunctions $\varphi_1 \vee \varphi_2 : z_k^{\ell, \varphi_1 \vee \varphi_2} = z_k^{\ell, \varphi_1} \vee z_k^{\ell, \varphi_2}$. (62)

- Always $\square_I \varphi : z_k^{\ell, \square_I \varphi} = \bigwedge_{k'=k_l}^{k_r} z_{k'}^{\ell, \varphi}$. (63)

- Eventually $\diamond_I \varphi : z_k^{\ell, \diamond_I \varphi} = \bigvee_{k'=k_l}^{k_r} z_{k'}^{\ell, \varphi}$. (64)

- Until $\varphi = \varphi_1 \mathcal{U} \varphi_2 :$

$$z_k^{\ell, \varphi} = \bigvee_{k'=k_l}^{k_r} \left(z_{k'}^{\ell, \varphi_2} \bigwedge \bigwedge_{k''=k}^{k'-1} z_{k''}^{\ell, \varphi_1} \right). \quad (65)$$

2) *Encoding Multi-Agent Collision Avoidance:* To ensure safety guarantees between any two agents i and j (where $1 \leq i < j \leq L$), the distance between their Bézier curves $B_k^i(t)$ and $B_k^j(t)$ is required to remain at least ϵ_{inter} for all $t \in [t_k, t_{k+1}]$. For simplicity, \mathcal{CH}_k^i and ϵ_k^i are grouped into the tuple $A_k^i = (\mathcal{CH}_k^i, \epsilon_k^i)$. Then, the multi-agent safety specification is defined as follows:

$$z_{\text{inter}} = \bigwedge_{1 \leq i < j \leq L} \text{safe} \left(A_k^i, A_k^j, \epsilon_{\text{inter}} \right), \quad (66)$$

where

$$\begin{aligned} \text{safe} \left(A_k^i, A_k^j, \epsilon_{\text{inter}} \right) &:= \|\text{cent}(B_k^i) - \text{cent}(B_k^j)\|_1 \\ &\geq \|c_{k,0}^i - c_{k,n}^i\|_1 + \|c_{k,0}^j - c_{k,n}^j\|_1 \\ &\quad + 2(\epsilon_k^i + \epsilon_k^j) + \epsilon_{\text{inter}} \sqrt{d}. \end{aligned} \quad (67)$$

and $\text{cent}(B_k^i) = \frac{1}{n+1} \sum_{l=0}^n c_{k,l}^i$ is the geometric center of the convex hull \mathcal{CH}_k^i .

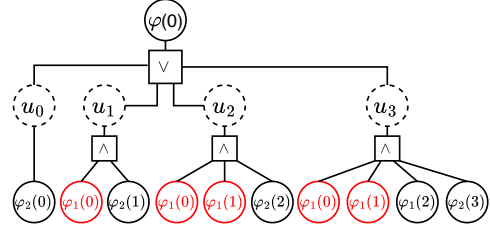
Lemma 1: If condition (67) holds for all agent pairs (i, j) with $1 \leq i < j \leq L$ over $t \in [t_k, t_{k+1}]$, then the distance between any two Bézier curves satisfies

$$\|B_k^i(t) - B_k^j(t)\| \geq \epsilon_{\text{inter}}. \quad (68)$$

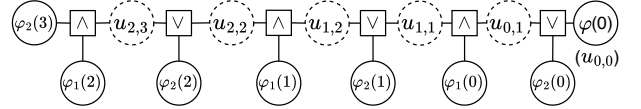
The proof can be seen in [Appendix III](#).

Remark 1: The multi-agent safety encoding is more restrictive because ensuring inter-agent safety requires the full convex hull of each Bézier curve. However, under acceleration constraints and with a limited number of control points, the resulting conservatism remains manageable. Moreover, the ℓ_1 -norm replaces the ℓ_2 -norm to yield convex and piecewise-linear formulations amenable to MICP solvers.

3) *Complexity Analysis:* Let $|\varphi|$ denote the number of disjunction occurrences in the STL formula φ , and let N_{win} denote the maximum temporal-window length measured in segment indices. For continuous-time STL specifications over piecewise Bézier trajectories with N segments, binary variables are introduced only for disjunctive operators. As shown in Fig. 3, the backward-recursion encoding reuses subformula encodings across parent operators, thereby avoiding the repeated encoding of overlapping subformulas. As a result, the total number of binary variables scales as $\mathcal{O}(N|\varphi|N_{\text{win}})$, whereas the direct semantic expansion scales as $\mathcal{O}(N|\varphi|N_{\text{win}}^2)$. For L agents with N Bézier segments, pairwise clearance constraints contribute $\mathcal{O}(L^2N)$ additional continuous constraints.



(a) Semantic expansion encoding. $\varphi(0) = \bigvee_{j=0}^3 u_j$ where $u_j = \varphi_2(j) \wedge \bigwedge_{i=0}^{j-1} \varphi_1(i)$, $j = \{0, 1, 2, 3\}$.



(b) Backward recursion encoding. $\varphi(0) = u_{0,0} = \varphi_2(0) \vee u_{0,1}$, where the auxiliary binary $u_{i,j}$ is indexed by i for $\varphi_1(i)$ and j for the witness $\varphi_2(j)$, and is updated via $u_{i,j} = \varphi_1(i) \wedge u_{i+1,j}$, $u_{i,j-1} = u_{i,j} \vee \varphi_2(j)$, for $i \in \{0, 1, 2\}$ and $j \in \{0, 1, 2, 3\}$.

Fig. 3: Two MICP encodings of $\varphi = (\varphi_1 \mathcal{U}_{[0,3]} \varphi_2)$ at time $t = 0$. Dashed circles denote auxiliary binary variables. The until window uses $N_{\text{win}} = 4$ discrete time steps with sampling interval $\Delta t = 1$. (a) The direct semantic expansion yields an $\mathcal{O}(N_{\text{win}}^2)$ -size encoding due to repeated occurrences of $\varphi_1(\cdot)$ (red circles). (b) The backward recursion shares subformulas and yields an $\mathcal{O}(N_{\text{win}})$ -size encoding.

VI. SIMULATIONS

This section evaluates the proposed framework on several benchmarks. The simulations are implemented in Python. Problem 1 is solved using differential evolution in SciPy [37], and Problem 2 is solved as an MICP using Gurobi [38]. All simulations are conducted on an 8-core Apple M1 machine with 16 GB of RAM.

A. Control Gains

The inertia matrix and mass of each quadrotor are $J = \text{diag}(8.20, 8.45, 13.77) \times 10^{-2} \text{ kg} \cdot \text{m}^2$ and $m = 4.34 \text{ kg}$, respectively, as given in [26]. The remaining parameters are $v_{\text{max}} = [3, 3, 3]^T$, $b_a = [1, 1, 11]^T$, and $\gamma_c = 0.2$.

To select the initial-condition parameters (42)–(44) in Proposition 2, Table II shows how individual variations in ψ_K , α_ψ , and \bar{V}_1 influence the peak position and velocity bounds, $\mathcal{L}_{\text{max},p} := \max_{t \in [0,T]} \mathcal{L}_p(t)$ and $\mathcal{L}_{\text{max},v} := \max_{t \in [0,T]} \mathcal{L}_v(t)$, as well as the initial-condition (IC) feasibility rate. The IC feasibility rate is defined as the percentage of feasible samples among 5000 samples drawn from the prescribed initial distributions, where $x_0, v_0 \sim \text{Unif}([-0.2, 0.2]^3)$, $\omega_0, \tau_0 \sim \text{Unif}([-0.1, 0.1]^3)$, and $R_0 = \exp(\tau_0)$. For each tuning case, one of ψ_K , α_ψ , and \bar{V}_1 is varied around the nominal setting $(\psi_K, \alpha_\psi, \bar{V}_1) = (0.05, 0.7, 0.4)$, while the other two parameters remain fixed.

Consistent with (42) and (43), Table II shows that increasing ψ_K enlarges the overall admissible rotational initial-condition set, thereby improving IC feasibility at the cost of looser peak bounds. By contrast, for a fixed ψ_K , α_ψ

mainly affects the relative strictness of the initial attitude and angular-velocity bounds. Table II indicates that α_ψ has a relatively mild effect on the peak bounds, whereas the IC feasibility rate varies noticeably. As for $\bar{\nu}_1$, increasing $\bar{\nu}_1$ enlarges the admissible translational initial-condition set, as expected from (44), and this is reflected in the higher IC feasibility reported in Table II, at the expense of larger peak bounds.

Overall, choosing $(\psi_K, \alpha_\psi, \bar{\nu}_1) = (0.05, 0.7, 0.4)$ provides a balance between IC feasibility and peak-bound conservatism. The optimized control gains are given by

$$K_p = \text{diag}(25.2, 24.6, 25.3), \quad K_v = \text{diag}(14.7, 14.7, 14.8), \\ K_R = \text{diag}(28.9, 27.9, 29.9), \quad K_\omega = \text{diag}(2.2, 1.8, 2.3),$$

and the auxiliary parameters are $\nu_1 = 0.75$ and $\nu_2 = 0.79$. Therefore, $\bar{\nu}_2 = 1.46$ is obtained from (45), yielding the maximum position and velocity error bounds $\mathcal{L}_{\max,p} = 0.61$ m and $\mathcal{L}_{\max,v} = 1.46$ m/s, respectively.

Furthermore, Table II shows that, compared with [26], the proposed method yields tighter error bounds in most cases, due to the additional tuning flexibility provided by multidimensional gain matrices.

TABLE II: Effects of individual variations of ψ_K , α_ψ , and $\bar{\nu}_1$ around the nominal setting $(0.05, 0.7, 0.4)$ on the peak bounds $\mathcal{L}_{\max,p}$, $\mathcal{L}_{\max,v}$, and the IC feasibility rate.

Params.	Value	$\mathcal{L}_{\max,p}$ (m)		$\mathcal{L}_{\max,v}$ (m/s)		IC Feasibility (%)	
		Proposed	[26]	Proposed	[26]	Proposed	[26]
ψ_K	0.005 ¹	0.37	0.36	0.77	0.72	12.20	13.02
	0.05	0.61 (Fig.5)	0.80	1.46	1.90	31.64	29.02
α_ψ	0.6	0.61	0.78	1.46	1.92	30.98	25.86
	0.8	0.60	0.80	1.43	1.92	31.42	27.56
$\bar{\nu}_1$	0.3	0.52	0.79	1.36	1.90	15.82	15.62
	0.5	0.69	0.80	1.54	1.91	52.28	41.42

¹ $\psi_K = 0.005$ follows $\bar{\Psi}$ in [26], as both characterize the allowable rotational initial error.

The following subsection presents four scenarios to validate the proposed method. Since multi-agent safety is already encoded in z_{inter} , it is omitted from the subsequent specifications. For readability, the statement that robot r avoids a region \mathbf{O} is denoted by $r \notin \mathbf{O}$, which is logically equivalent to the negation $\neg(r \in \mathbf{O})$.

B. Case 0: Runtime Analysis

To evaluate how runtime scales with the number of agents, we consider the simple scenario shown in Fig. 4. Because this scenario is simple and can accommodate different numbers of quadrotors, it better isolates the effect of L on computation time. The specification is

$$\varphi = \bigwedge_{\ell=1}^L (\square_{[0,T]}(r_\ell \notin \mathbf{Y})) \wedge (\diamond_{[0,T]} r_\ell \in \mathbf{B}), \quad (69)$$

which requires the robots to avoid the yellow obstacle \mathbf{Y} and reach the blue region \mathbf{B} . Table III shows that runtime increases with the number of agents L , consistent with the $\mathcal{O}(L^2N)$ scaling of pairwise collision-avoidance constraints

discussed in Section V-B.3. The runtime is compared against the MICP baseline proposed in [32], which uses direct semantic expansions and Bézier-curve trajectory parameterization. To enable a fair comparison in the multi-agent setting, the same collision-avoidance encoding is also incorporated into the baseline. As the number of robots L increases, the proposed method shows lower runtime than the baseline. This is due to the backward-recursive encoding of temporal operators, which avoids the quadratic blow-up associated with witness-based semantic expansions.

TABLE III: Runtime (seconds) comparison in terms of the number of robots.

#Robots	The proposed	MICP [32]
2	0.16	0.91
3	1.17	5.56
4	8.79	27.20
5	17.89	73.80
6	54.42	171.98

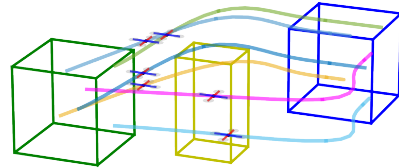


Fig. 4: Case 0 environment with six quadrotors ($L = 6$).

C. Case 1: Narrow Corridors

In Case 1, the quadrotors are required to fly through a continuously narrowing passage away from the five yellow $\{\mathbf{Y}_i\}_{i=1}^5$, and eventually reach a compact blue region \mathbf{B} , as shown in Fig. 5(a)–(c). The navigation constraints are getting progressively tighter. Given $T = 17$ s, the specification is

$$\varphi = \bigwedge_{\ell=1}^2 \left((\wedge_{i=1}^5 \square_{[0,T]}(r_\ell \notin \mathbf{Y}_i)) \wedge (\diamond_{[0,T]} r_\ell \in \mathbf{B}) \right). \quad (70)$$

D. Case 2: Reach and Avoid

Case 2 requires each quadrotor r_ℓ to stay away from the yellow obstacles \mathbf{Y} and remain in the green region \mathbf{G} for at least 2 seconds. Finally, all quadrotors need to reach the diagonally opposite blue region, as depicted in Fig. 5(e)–(g), resulting in an interlaced routing challenge. Given $T = 20$ s, the specification is

$$\varphi = \bigwedge_{\ell=1}^4 \left((\square_{[0,T]}(r_\ell \notin \mathbf{Y})) \wedge (\diamond_{[0,T]} \square_{[0,2]} r_\ell \in \mathbf{G}) \wedge (\diamond_{[0,T]} r_\ell \in \mathbf{B}^{\ell'}) \right), \quad (71)$$

where the pairing $(\ell, \ell') \in \{(1, 3), (2, 4), (3, 1), (4, 2)\}$ encodes this diagonal goal assignment.

E. Case 3: Key–Door Puzzle

In Case 3, robot r_1 must first retrieve the key in the purple region \mathbf{K} to unlock the green gate \mathbf{G} . Only then can both robots reach the blue target region \mathbf{R} by passing through \mathbf{G} while avoiding the yellow walls \mathbf{Y} , as shown in Fig. 5(i)–(k). Here, with $T = 20$, the specification is expressed as

$$\varphi = (r_2 \notin \mathbf{G}) \mathcal{U}_{[0,T]} ((r_1 \notin \mathbf{G}) \mathcal{U}_{[0,T]} (r_1 \in \mathbf{K})) \bigwedge_{\ell=1}^2 ((\diamond_{[0,T]} r_\ell \in \mathbf{R}) \wedge (\square_{[0,T]} r_\ell \notin \mathbf{Y})). \quad (72)$$

This specification is complex due to the nested structure of the two *Until* operators.

In all cases mentioned above, the Bézier trajectories are parameterized by eight control points ($n = 8$), and the tracking time step is $dt = 0.2$ s. For each case, the planned trajectories y_d^ℓ and the corresponding tracking trajectories y_{tr}^ℓ are generated for all agents ℓ . For each approach, 100 tracking trials per agent are simulated under identical initial error conditions. The experimental results are analyzed in terms of stability, safety, and robustness.

F. Stability Analysis

Table IV illustrates the comparison of the stability performance of the proposed method and that of [26]. The position error convergence time $t_{c,p}$ is defined as the earliest time such that $\|e_p(t)\| \leq 10^{-2}$ m for all $t \geq t_{c,p}$. Similarly, the velocity error convergence time $t_{c,v}$ is defined as the earliest time such that $\|e_v(t)\| \leq 10^{-2}$ m/s for all $t \geq t_{c,v}$. The post-convergence errors \bar{e}_p and \bar{e}_v are defined as the means of all finite samples of $\|e_p(t)\|$ for $t \geq t_{c,p}$ and $\|e_v(t)\|$ for $t \geq t_{c,v}$, respectively, pooled over all agents and trajectories in each case.

As shown in the fourth column of Fig. 5, the proposed controller yields lower time-varying mean errors $\|e_p(t)\|$ and $\|e_v(t)\|$, together with narrower shaded bands, indicating smaller dispersion across trials over time. Because the post-convergence behavior is not directly evident in Fig. 5, the convergence times and post-convergence errors in Table IV show that the proposed method achieves faster transients, tighter steady-state tracking, and reduced residual oscillations relative to the scalar-gain baseline [26].

Table IV also lists the computation time. Although the proposed controller employs vector-valued gains, its faster transient response enables more efficient tracking and leads to a lower computation time for completing a reference trajectory. Overall, the proposed approach improves both tracking performance and computational efficiency.

G. Safety and Robustness Analysis

Safety is assessed by examining both the planning and tracking trajectories. A safety threshold of $\epsilon_{\text{inter}} = 0.2$ m, equal to γ_c , is enforced on the minimum inter-trajectory distance. As reported in Table V, the minimum inter-trajectory distances are evaluated over the discrete time $\mathcal{T} =$

$\{t_k = kdt \mid 0 \leq kdt \leq T\}$. The minimum distance between planning trajectories is defined as

$$\text{dist}_{\text{plan}} = \min_{1 \leq i < j \leq L} \min_{t_k \in \mathcal{T}} \|y_d^i(t_k) - y_d^j(t_k)\|. \quad (73)$$

The tracking distance $\text{dist}_{\text{track}}$ is the overall minimum inter-trajectory distance over all time steps in \mathcal{T} , across all agents and all tracking trials (100 per agent). Table V shows that, in all cases, the minimum inter-trajectory distances exceed the safety threshold ϵ_{inter} , thereby ensuring collision-free behavior during both planning and tracking. Moreover, the worst-case robustness across all robots is $\rho_{\text{min}}^\varphi = 0.3 > 0$, confirming that all Bézier trajectories satisfy the STL specifications. Meanwhile, Fig. 5 displays that $\rho_{\text{min}}^\varphi(t) \geq \bar{L}_p(t) = \Gamma(t)$ for all $t \in [0, T]$, implying that the tracked trajectories also satisfy the STL specifications according to (17).

VII. CONCLUSION

This paper presents a continuous-time control framework for multi-quadrotor systems under STL specifications by integrating geometric tracking control with MICP-based Bézier trajectory generation. The proposed approach enables safe and dynamically feasible motion planning with formal tracking guarantees. Compared with conventional scalar-gain designs, the matrix-gain geometric controller yields tighter tracking bounds and improved tracking performance. In addition, the multi-agent extension of the continuous-time STL Bézier planning framework improves computational efficiency while ensuring specification satisfaction. However, the method still relies on accurate models and suitable initial tracking conditions, and its computational burden increases with the number of agents. Future work includes distributed implementations for improved scalability, extensions to SE(3) curve planning for full-pose coordination, and the integration of learning-based methods for enhanced adaptability.

REFERENCES

- [1] Graeme Best, Rohit Garg, John Keller, Geoffrey A Hollinger, and Sebastian Scherer. Multi-robot, multi-sensor exploration of multifarious environments with full mission aerial autonomy. *The International Journal of Robotics Research*, 43(4):485–512, 2024.
- [2] Calin Belta and Sadra Sadraddini. Formal methods for control synthesis: An optimization perspective. *Annual Review of Control, Robotics, and Autonomous Systems*, 2(1):115–140, 2019.
- [3] Dawei Sun, Jingkai Chen, Sayan Mitra, and Chuchu Fan. Multi-agent motion planning from signal temporal logic specifications. *IEEE Robotics and Automation Letters*, 7(2):3451–3458, 2022.
- [4] Yash Vardhan Pant, Houssam Abbas, Rhudii A Quaye, and Rahul Mangharam. Fly-by-logic: Control of multi-drone fleets with temporal logic objectives. In *2018 ACM/IEEE 9th International Conference on Cyber-Physical Systems (ICCPs)*, pages 186–197. IEEE, 2018.
- [5] Yuanyuan Zou, Xu Su, Shaoyuan Li, Yugang Niu, and Dewei Li. Event-triggered distributed predictive control for asynchronous coordination of multi-agent systems. *Automatica*, 99:92–98, 2019.
- [6] Xiaoyi Zhou, Yuanyuan Zou, Shaoyuan Li, Xianwei Li, and Hao Fang. Distributed model predictive control for multi-robot systems with conflicting signal temporal logic tasks. *IET Control Theory & Applications*, 16(5):554–572, 2022.
- [7] Ali Tefvik Büyükköçak, Derya Aksaray, and Yasin Yazicioglu. Distributed planning of multi-agent systems with coupled temporal logic specifications. In *AIAA Scitech 2021 Forum*, page 1123, 2021.

TABLE IV: Tracking performance comparison between the proposed method and [26], reported as mean \pm std over pooled trajectories from all agents in each case. Here, $t_{c,p}$ and $t_{c,v}$ are the position and velocity error convergence times, respectively.

Case	Computation time (s)		Convergence time $t_{c,p}$ (s)		$\bar{e}_p \pm \sigma_p (\times 10^{-3} \text{ m})$		Convergence time $t_{c,v}$ (s)		$\bar{e}_v \pm \sigma_v (\times 10^{-3} \text{ m/s})$	
	The proposed	[26]	The proposed	[26]	The proposed	[26]	The proposed	[26]	The proposed	[26]
Narrow Corridors	0.54 \pm 0.03	0.60 \pm 0.02	1.57 \pm 0.24	4.41 \pm 0.36	0.60 \pm 0.07	1.73 \pm 0.10	2.10 \pm 0.24	5.38 \pm 0.32	0.76 \pm 0.14	2.29 \pm 0.01
Reach-Avoid	0.48 \pm 0.02	0.52 \pm 0.03	1.57 \pm 0.23	4.33 \pm 0.39	0.38 \pm 0.04	1.02 \pm 0.08	2.10 \pm 0.23	5.89 \pm 0.49	0.40 \pm 0.10	1.2 \pm 0.21
Key-Door	0.52 \pm 0.08	0.57 \pm 0.05	1.58 \pm 0.24	4.34 \pm 0.44	0.37 \pm 0.02	0.97 \pm 0.01	2.11 \pm 0.24	5.91 \pm 0.48	0.37 \pm 0.04	1.1 \pm 0.01

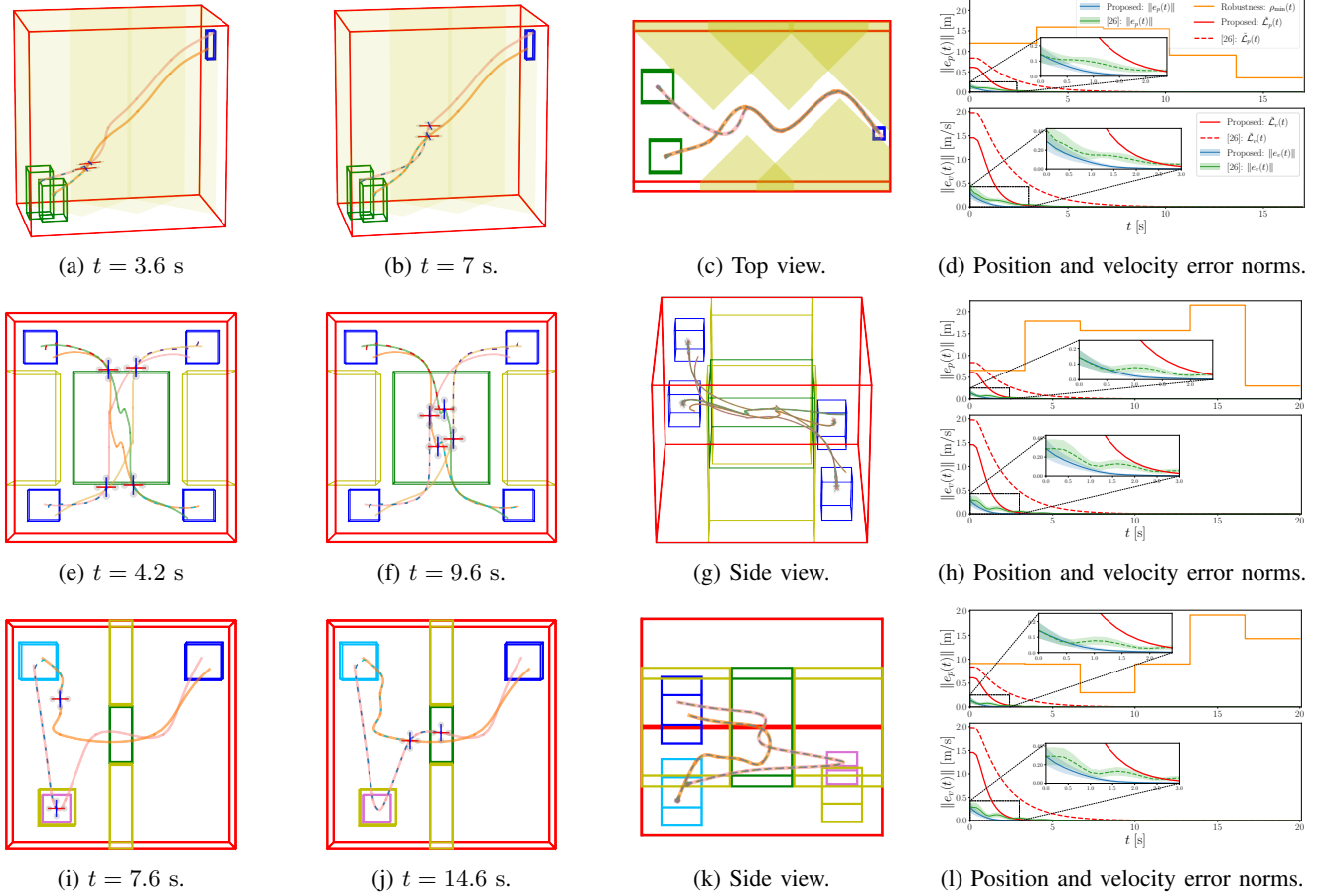


Fig. 5: Benchmarks and results for Cases 1–3 (top to bottom). In the environment plots, solid lines denote planned trajectories and dashed lines denote tracking trajectories. Columns 1–2 show two representative time snapshots (only the trajectory with the largest $\|e_p\|$ is plotted for clarity), Column 3 shows additional views and tracking trajectories, and Column 4 compares the position and velocity tracking errors and their corresponding bounds for the proposed method and [26].

TABLE V: Safety summary across cases: number of robots (ℓ), number of segments (#S), worst-case robustness margin $\rho_{\min}^{\varphi} = \min_{1 \leq \ell \leq L} \min_{t_k \in \mathcal{T}} \rho^{\ell, \varphi}(t_k)$, and minimum inter-trajectory distances from planned ($\text{dist}_{\text{plan}}$) and tracking ($\text{dist}_{\text{track}}$) trajectories.

Case	ℓ	#S	Runtime(s)	ρ_{\min}^{φ}	$\text{dist}_{\text{plan}}$	$\text{dist}_{\text{track}}$
Narrow Corridors	4	5	0.07	0.3	0.615	0.616
Reach-Avoid	2	6	11.92	0.3	0.462	0.461
Key-Door	2	6	1.28	0.3	0.773	0.772

- [8] Maria Charitidou and Dimos V Dimarogonas. Distributed MPC with continuous-time STL constraint satisfaction guarantees. *IEEE Control Systems Letters*, 8:211–216, 2024.
- [9] Georgios E Fainekos and George J Pappas. Robustness of temporal logic specifications. In *International Workshop on Formal Approaches to Software Testing*, pages 178–192. Springer, 2006.
- [10] Yash Vardhan Pant, Houssam Abbas, and Rahul Mangharam. Smooth operator: Control using the smooth robustness of temporal logic. In *2017 IEEE Conference on Control Technology and Applications (CCTA)*, pages 1235–1240, 2017.
- [11] Yann Gilpin, Vince Kurtz, and Hai Lin. A smooth robustness measure of signal temporal logic for symbolic control. *IEEE Control Systems Letters*, 5(1):241–246, 2020.

- [12] Lars Lindemann and Dimos V Dimarogonas. Decentralized control barrier functions for coupled multi-agent systems under signal temporal logic tasks. In *Proc. of ECC*, pages 89–94. IEEE, 2019.
- [13] Maryam Sharifi and Dimos V Dimarogonas. Fixed-time convergent control barrier functions for coupled multi-agent systems under STL tasks. In *Proc. of ECC*, pages 793–798. IEEE, 2021.
- [14] Nishanth Rao, Suresh Sundaram, and Pushpak Jagtap. Temporal waypoint navigation of multi-UAV payload system using barrier functions. In *Proc. of ECC*, pages 1–6. IEEE, 2023.
- [15] Xiangwei Bu. Prescribed performance control approaches, applications and challenges: A comprehensive survey. *Asian Journal of Control*, 25(1):241–261, 2023.
- [16] Lars Lindemann, Christos K Verginis, and Dimos V Dimarogonas. Prescribed performance control for signal temporal logic specifications. In *Proc. of CDC*, pages 2997–3002. IEEE, 2017.
- [17] Fei Chen and Dimos V Dimarogonas. Funnell-based cooperative control of leader-follower multi-agent systems under signal temporal logic specifications. In *Proc. of ECC*, pages 906–911. IEEE, 2022.
- [18] Siyuan Liu, Adnane Saoud, and Dimos V Dimarogonas. Controller synthesis of collaborative signal temporal logic tasks for multi-agent systems via assume-guarantee contracts. *IEEE Transactions on Automatic Control*, 2025.
- [19] Chuchu Fan, Kristina Miller, and Sayan Mitra. Fast and guaranteed safe controller synthesis for nonlinear vehicle models. In *Computer Aided Verification*, pages 629–652, Cham, 2020. Springer International Publishing.
- [20] Yash Vardhan Pant, He Yin, Murat Arcak, and Sanjit A. Seshia. Co-design of control and planning for multi-rotor UAVs with signal temporal logic specifications. In *Proc. of ACC*, pages 4209–4216, 2021.
- [21] Weibin Gu, Stefano Primatesta, and Alessandro Rizzo. Robust adaptive control for aggressive quadrotor maneuvers via SO(3) and backstepping techniques. *Robotics and Autonomous Systems*, page 104942, 2025.
- [22] Taeyoung Lee, Melvin Leok, and N Harris McClamroch. Geometric tracking control of a quadrotor UAV on SE(3). In *Proc. of CDC*, pages 5420–5425. IEEE, 2010.
- [23] Taeyoung Lee. Robust adaptive attitude tracking on SO(3) with an application to a quadrotor UAV. *IEEE Transactions on Control Systems Technology*, 21(5):1924–1930, 2012.
- [24] Davide Invernizzi and Marco Lovera. Geometric tracking control of a quadcopter tiltrotor UAV. *IFAC-PapersOnLine*, 50(1):11565–11570, 2017.
- [25] Kanishke Gamagedara, Mahdis Bisheban, Evan Kaufman, and Taeyoung Lee. Geometric controls of a quadrotor UAV with decoupled yaw control. In *Proc. of ACC*, pages 3285–3290. IEEE, 2019.
- [26] Mohamed Serry, Yating Yuan, Haocheng Chang, and Jun Liu. Reach-avoid control synthesis for a quadrotor uav with formal safety guarantees. *IEEE Transactions on Automatic Control*, pages 1–15, 2026.
- [27] Pian Yu, Xiao Tan, and Dimos V Dimarogonas. Continuous-time control synthesis under nested signal temporal logic specifications. *IEEE Transactions on Robotics*, 2024.
- [28] Karen Leung, Nikos Aréchiga, and Marco Pavone. Backpropagation through signal temporal logic specifications: Infusing logical structure into gradient-based methods. *The International Journal of Robotics Research*, 42(6):356–370, 2023.
- [29] Kevin M. Lynch and Frank C. Park. *Modern Robotics: Mechanics, Planning, and Control*. Cambridge University Press, 2017.
- [30] Sadra Sadraddini and Calin Belta. Robust temporal logic model predictive control. In *2015 53rd Annual Allerton Conference on Communication, Control, and Computing (Allerton)*, pages 772–779. IEEE, 2015.
- [31] Alexandre Donzé and Oded Maler. Robust satisfaction of temporal logic over real-valued signals. In *Proc. of FORMATS*, 2010.
- [32] Yating Yuan, Thanin Quartz, and Jun Liu. Signal temporal logic planning with time-varying robustness. *IEEE Control Systems Letters*, 2024.
- [33] Roger A. Horn and Charles R. Johnson. *Matrix Analysis*. Cambridge University Press, 2 edition, 2012.
- [34] Hassan K Khalil and Jessy W Grizzle. *Nonlinear systems*, volume 3. Prentice hall Upper Saddle River, NJ, 2002.
- [35] Richard M Murray, Zexiang Li, and S Shankar Sastry. *A mathematical introduction to robotic manipulation*. CRC press, 2017.
- [36] Rainer Storn and Kenneth Price. Differential evolution—a simple and efficient heuristic for global optimization over continuous spaces. *Journal of global optimization*, 11(4):341–359, 1997.
- [37] Pauli Virtanen, Ralf Gommers, Travis E. Oliphant, Matt Haberland, Tyler Reddy, David Cournapeau, Evgeni Burovski, Pearu Peterson, Warren Weckesser, Jonathan Bright, Stéfan J. van der Walt, Matthew Brett, Joshua Wilson, K. Jarrod Millman, Nikolay Mayorov, Andrew R. J. Nelson, Eric Jones, Robert Kern, Eric Larson, C J Carey, İlhan Polat, Yu Feng, Eric W. Moore, Jake VanderPlas, Denis Laxalde, Josef Perktold, Robert Cimrman, Ian Henriksen, E. A. Quintero, Charles R. Harris, Anne M. Archibald, Antônio H. Ribeiro, Fabian Pedregosa, Paul van Mulbregt, and SciPy 1.0 Contributors. SciPy 1.0: Fundamental Algorithms for Scientific Computing in Python. *Nature Methods*, 17:261–272, 2020.
- [38] Gurobi Optimizer Reference Manual, 2024.

I. PROOF OF LYAPUNOV BOUNDS

The proof of the Lyapunov bounds is based on the following error dynamics and on Lemmas 2 and 3, whose proofs are given in Appendix V and Appendix VI, respectively.

For all $t \in \mathbb{T}$, let $G(t) := R_d^\top(t)R(t) \in \text{SO}(3)$, and the error dynamics for (6)–(10) are as follows.

$$\dot{e}_p(t) = e_v(t), \quad (\text{I.1})$$

$$\dot{e}_v(t) = -\frac{1}{m}(K_p e_p(t) + K_v e_v(t) - \Delta_f(t)), \quad (\text{I.2})$$

$$\dot{\Psi}_K(t) = e_{K,R}^\top(t)e_\omega(t), \quad (\text{I.3})$$

$$\dot{e}_{K,R}(t) = \mathcal{C}(t)e_\omega(t), \quad (\text{I.4})$$

$$\dot{e}_\omega(t) = -J^{-1}(e_{K,R}(t) + K_\omega e_\omega(t)), \quad (\text{I.5})$$

where

$$\mathcal{C}(t) := \frac{1}{2}(\text{tr}[K_R G(t)]I_3 - K_R G(t)), \quad (\text{I.6})$$

$$\Delta_f(t) = \|F_d(t)\| \left((b_{3,d}^\top(t)b_3(t) - b_{3,d}(t)) \right). \quad (\text{I.7})$$

The detailed derivation of the above error dynamics is given in Appendix IV.

Lemma 2 ([23, Proposition 2]): For all $t \in \mathbb{T}$,

$$\|\mathcal{C}(t)\| \leq \frac{1}{\sqrt{2}}\text{tr}[K_R]. \quad (\text{I.8})$$

Lemma 3: Suppose $K_R = \text{diag}(k_{R_1}, k_{R_2}, k_{R_3}) \in \mathbb{S}_{++}^3$ and $\Psi_K(t) < \psi < h_1$. Then,

$$\|b_{3,d} - b_{3,d}^\top b_3 b_3\| \leq \sqrt{\frac{4g_2}{h_1}} \|e_{K,R}\|. \quad (\text{I.9})$$

which further implies that

$$\|\Delta_f\| \leq \left(\| [K_p \ K_v] M_1^{-1/2} \| \sqrt{\mathcal{V}_1} + m \|b_a\| \right) \sqrt{\frac{4g_2}{h_1}} \|e_{K,R}\|. \quad (\text{I.10})$$

By (I.3)–(I.5), the time derivative of $\mathcal{V}_2(t)$ in (27) is

$$\dot{\mathcal{V}}_2(t) = -c_2 e_{K,R}^\top(t) J^{-1} e_{K,R}(t) - c_2 e_\omega^\top(t) K_\omega J^{-1} e_{K,R}(t) - e_\omega^\top(t) (K_\omega - c_2 \mathcal{C}) e_\omega(t). \quad (\text{I.11})$$

Let $z_2^\top(t) := [e_{K,R}^\top(t) \ e_\omega^\top(t)]$. Then, by Lemma 2 and the definitions of W_2 and β in (32) and (34), it follows that

$$\dot{\mathcal{V}}_2(t) \leq -z_2^\top(t) W_2 z_2(t) \leq -\beta \mathcal{V}_2(t). \quad (\text{I.12})$$

By the comparison principle in [34, Section 3.4],

$$\sqrt{\mathcal{V}_2(t)} \leq e^{-\beta t/2} \sqrt{\mathcal{V}_2(0)}. \quad (\text{I.13})$$

Also, since $z_2^\top M_{2,1} z_2 \leq \mathcal{V}_2$, there is

$$\|e_{K,R}(t)\| \leq \left\| [I_3 \ 0] M_{2,1}^{-1/2} \right\| \sqrt{\mathcal{V}_2(t)}. \quad (\text{I.14})$$

Let $z_1^\top(t) := [e_p^\top(t) \ e_v^\top(t)]$. Given $\alpha_0, \alpha_1, \alpha_2$ and β' defined in (37)–(40), let $C_1 := \begin{bmatrix} c_1 I_3 & I_3 \end{bmatrix}$. Using (I.1), (I.2), and Lemma 3, the time derivative of $\mathcal{V}_1(t)$ in (21) is

$$\begin{aligned} \dot{\mathcal{V}}_1(t) &= -z_1^\top(t) W_1 z_1(t) - \Delta_f^\top(t) C_1 z_1(t) \\ &\leq -\alpha_0 \mathcal{V}_1(t) + \|\Delta_f(t)\| \|C_1 z_1(t)\|. \end{aligned} \quad (\text{I.15})$$

From (21), it follows that $\|C_1 z_1(t)\| \leq \|C_1 M_1^{-1/2}\| \sqrt{\mathcal{V}_1(t)}$. By (I.10) and (I.14),

$$\|\Delta_f(t)\| \|C_1 z_1(t)\| \leq \alpha_1 \sqrt{\mathcal{V}_2(t)} \mathcal{V}_1(t) + \alpha_2 \sqrt{\mathcal{V}_2(t)} \mathcal{V}_1(t). \quad (\text{I.16})$$

Substituting (I.16) into (I.15) and using (I.13) yields

$$\begin{aligned} \dot{\mathcal{V}}_1(t) &\leq -(\alpha_0 - \alpha_1 e^{-\beta t/2} \sqrt{\mathcal{V}_2(0)}) \mathcal{V}_1(t) \\ &\quad + \alpha_2 e^{-\beta t/2} \sqrt{\mathcal{V}_2(0)} \sqrt{\mathcal{V}_1(t)}. \end{aligned} \quad (\text{I.17})$$

Applying the comparison principle in [34, Section 3.4] again yields

$$\sqrt{\mathcal{V}_1(t)} \leq \mathcal{L}_1(\mathcal{V}_1(0), \mathcal{V}_2(0), t), \quad (\text{I.18})$$

where

$$\begin{aligned} \mathcal{L}_1(\mathcal{V}_1(0), \mathcal{V}_2(0), t) &= e^{-\alpha_0 t/2} \left[e^{\alpha_1 \sqrt{\mathcal{V}_2(0)}/\beta} \sqrt{\mathcal{V}_1(0)} \right. \\ &\quad \left. + \frac{\alpha_2 \sqrt{\mathcal{V}_2(0)}}{2} \int_0^t e^{(\alpha_0 - \beta)s/2} ds \right]. \end{aligned} \quad (\text{I.19})$$

II. PROOF OF INITIAL CONDITIONS

Define $\mathcal{E}(t) := \frac{1}{2} e_\omega^\top(t) J e_\omega(t) + \Psi_K(t)$. With (I.3) and (I.5), it follows that

$$\dot{\mathcal{E}}(t) = e_\omega^\top(t) J \dot{e}_\omega(t) + \dot{\Psi}_K(t) = -e_\omega^\top(t) K_\omega e_\omega(t). \quad (\text{II.1})$$

Since $J, K_\omega \in \mathbb{S}_{++}^3$, $\dot{\mathcal{E}}(t) \leq 0$, which implies that $\dot{\Psi}_K(t) \leq 0$. With the initial conditions (42) and (43), it holds that

$$\mathcal{E}(0) = \frac{1}{2} e_\omega^\top(0) J e_\omega(0) + \Psi_K(0) < \psi < h_1. \quad (\text{II.2})$$

This indicates that $\Psi_K(t) \leq \Psi_K(0) < \psi < h_1$ for all $t \geq 0$. Hence, this condition of Proposition 1 and Lemma 3 holds. Given $g_1 \|e_{K,R}(0)\|^2 \leq \Psi_K(0)$ from Proposition 1, and by $\mathcal{V}_2(t)$ in (27), one has

$$\begin{aligned} \mathcal{V}_2(0) &= \frac{1}{2} e_\omega^\top(0) J e_\omega(0) + \Psi_K(0) + c_2 e_{K,R}^\top(0) e_\omega(0) \\ &\leq (1 - \alpha_\psi) \psi + \alpha_\psi \psi + c_2 \|e_{K,R}(0)\| \|e_\omega(0)\| \\ &\leq \psi + c_2 \sqrt{\frac{\psi}{g_1}} \left\| J^{-1/2} \right\| \left\| J^{1/2} e_\omega(0) \right\| \\ &\leq \left(1 + c_2 \sqrt{\frac{2(1 - \alpha_\psi) \alpha_\psi}{\lambda(J) g_1}} \right) \psi = \bar{\mathcal{V}}_2. \end{aligned} \quad (\text{II.3})$$

Therefore, with $\mathcal{V}_1(0) \leq \bar{\mathcal{V}}_1$ in (44) and $\mathcal{V}_2(0) \leq \bar{\mathcal{V}}_2$, one has $\mathcal{L}_1(\mathcal{V}_1(0), \mathcal{V}_2(0), t) \leq \mathcal{L}_1(\bar{\mathcal{V}}_1, \bar{\mathcal{V}}_2, t)$. From (21) and (I.18),

$$\begin{aligned} \|e_p(t)\| &= \left\| [I_3 \ 0_{3 \times 3}] M_1^{-\frac{1}{2}} M_1^{\frac{1}{2}} z_1(t) \right\| \\ &\leq \left\| [I_3 \ 0_{3 \times 3}] M_1^{-\frac{1}{2}} \right\| \sqrt{\mathcal{V}_1(t)} \\ &\leq \left\| [I_3 \ 0_{3 \times 3}] M_1^{-\frac{1}{2}} \right\| \mathcal{L}_1(\bar{\mathcal{V}}_1, \bar{\mathcal{V}}_2, t) = \mathcal{L}_p(t). \end{aligned} \quad (\text{II.4})$$

Likewise, the bound of $\|e_v(t)\|$ can be derived as

$$\|e_v(t)\| \leq \left\| [0_{3 \times 3} \ I_3] M_1^{-\frac{1}{2}} \right\| \mathcal{L}_1(\bar{\mathcal{V}}_1, \bar{\mathcal{V}}_2, t) = \mathcal{L}_v(t). \quad (\text{II.5})$$

APPENDIX III. MULTI-AGENT COLLISION AVOIDANCE

The radius (or span) of the k -th Bézier segment B_k^i of the i -th agent quantifies that segment's spatial extent (compactness) and is defined as the maximum Euclidean distance between its geometric centroid, $\text{cent}(B_k^i)$, and any of its control points:

$$\text{span}(B_k^i) = \max_{0 \leq l \leq n} \|c_{k,l}^i - \text{cent}(B_k^i)\|, \quad (\text{III.1})$$

where $\text{cent}(B_k^i) = \frac{1}{n+1} \sum_{l=0}^n c_{k,l}^i$. From constraints (60), it is proved in [32] that, for $\forall l \in \{1, 2, \dots, n\}$,

$$\min \{ \|c_{k,l}^i - c_{k,0}^i\|, \|c_{k,l}^i - c_{k,n}^i\| \} \leq \epsilon_k^i, \quad (\text{III.2})$$

which illustrates that every control point $c_{k,l}^i$ is close to at least one of the endpoints $c_{k,0}^i$ or $c_{k,n}^i$. Denote $m_k^* = (c_{k,0}^i + c_{k,n}^i)/2$ as the midpoint of the segment connecting the endpoints. Without loss of generality, assume that $c_{k,l}^i$ is closer to $c_{k,0}^i$ than to $c_{k,n}^i$. Then,

$$\begin{aligned} \|c_{k,l}^i - m_k^*\| &\leq \|c_{k,l}^i - c_{k,0}^i\| + \|c_{k,0}^i - m_k^*\| \\ &= \epsilon_k^i + \frac{1}{2} \|c_{k,0}^i - c_{k,n}^i\|. \end{aligned} \quad (\text{III.3})$$

The same holds if closer to $c_{k,n}^i$. Therefore,

$$\begin{aligned} \|\text{cent}(B_k^i) - m_k^*\| &= \left\| \frac{1}{n+1} \sum_{l=0}^n c_{k,l}^i - m_k^* \right\| \\ &\leq \epsilon_k + \frac{1}{2} \|c_{k,0}^i - c_{k,n}^i\| \end{aligned} \quad (\text{III.4})$$

Thus, for any control point $c_{k,l}^i$,

$$\begin{aligned} \|c_{k,l}^i - \text{cent}(B_k^i)\| &\leq \|c_{k,l}^i - m_k^*\| + \|\text{cent}(B_k^i) - m_k^*\| \\ &\leq 2\epsilon_k^i + \|c_{k,0}^i - c_{k,n}^i\|. \end{aligned} \quad (\text{III.5})$$

yielding $\text{span}(B_k^i) \leq 2\epsilon_k^i + \|c_{k,0}^i - c_{k,n}^i\|$. since any point at the Bézier curve $B_k^i(t)$ is within the convex hull, $\|B_k^i(t) - \text{cent}(B_k^i)\| \leq \text{span}(B_k^i)$.

Consider any two Bézier curves B_k^i and B_k^j over $t \in [t_k, t_{k+1}]$, with convex hulls $\mathcal{CH}_k^i = \{c_{k,l}^i\}_{l=0}^n$ and $\mathcal{CH}_k^j = \{c_{k,l}^j\}_{l=0}^n$. The constraint (67) implies that

$$\begin{aligned} \|\text{cent}(B_k^i) - \text{cent}(B_k^j)\|_1 &\geq 2\epsilon_k^i + \|c_{k,0}^i - c_{k,n}^i\|_1 + 2\epsilon_k^j \\ &\quad + \|c_{k,0}^j - c_{k,n}^j\|_1 + \epsilon_{inter} \sqrt{d} \\ &\geq \text{span}(B_k^i) + \text{span}(B_k^j) + (\epsilon_{inter} \sqrt{d}). \end{aligned} \quad (\text{III.6})$$

Then, by the triangle inequality, for any $t \in [t_k, t_{k+1}]$,

$$\begin{aligned} \|B_k^i(t) - B_k^j(t)\|_1 &\geq \|\text{cent}(B_k^i) - \text{cent}(B_k^j)\|_1 \\ &\quad - \text{span}(B_k^i) - \text{span}(B_k^j) \quad (\text{III.7}) \\ &\geq \epsilon_{\text{inter}} \sqrt{d}. \end{aligned}$$

By the norm inequality $\|x\|_1 \leq \sqrt{d}\|x\|$, it follows that,

$$\|B_k^i(t) - B_k^j(t)\| \geq \epsilon_{\text{inter}}. \quad (\text{III.8})$$

APPENDIX IV. ERROR DYNAMICS

Given the error functions (6)–(10), their time derivatives are derived as follows.

• **The derivative of $e_p(t)$:**

$$\dot{e}_p(t) = \dot{y}_{tr}(t) - \dot{y}_d(t) = e_v(t). \quad (\text{V.1})$$

• **The derivative of $e_v(t)$:** From (2) and (19), one has

$$\begin{aligned} m\dot{e}_v(t) &= m\dot{y}_{tr}(t) - m\dot{y}_d(t) \\ &= -(K_p e_p(t) + K_v e_v(t)) - (F_d(t) - f(t)R(t)e_3). \quad (\text{V.2}) \end{aligned}$$

Since $f(t) = F_d^\top(t)R(t)e_3$, $b_3(t) = R(t)e_3$, and $b_{3,d}(t) = \frac{F_d(t)}{\|F_d(t)\|}$, it follows that

$$\begin{aligned} f(t)R(t)e_3 - F_d(t) &= (F_d^\top(t)b_3(t))b_3(t) - \|F_d(t)\|b_{3,d}(t) \\ &= \|F_d(t)\|(b_{3,d}^\top(t)b_3(t))b_3(t) - \|F_d(t)\|b_{3,d}(t) \\ &\triangleq \Delta_f(t). \quad (\text{V.3}) \end{aligned}$$

Thus, $\dot{e}_v(t) = -\frac{1}{m}(K_p e_p(t) + K_v e_v(t) - \Delta_f(t))$.

• **The derivative of $\Psi_K(t)$:** Let $G(t) = R_d^\top(t)R(t) \in \text{SO}(3)$. Given $\hat{\omega}_d(t) \in \mathfrak{so}(3)$, the following properties hold:

$$\hat{\omega}_d^\top(t) = -\hat{\omega}_d(t) \quad (\text{V.4})$$

$$G(t)G^\top(t) = 1 \quad (\text{V.5})$$

$$G^\top(t)\hat{\omega}_d(t)G(t) = (G^\top(t)\omega_d(t))^\wedge. \quad (\text{V.6})$$

Using these properties and the definition of $e_\omega(t)$, one has

$$\begin{aligned} \dot{G}(t) &= \dot{R}_d^\top(t)R(t) + R_d^\top(t)\dot{R}(t) \\ &= -\hat{\omega}_d(t)G(t) + G(t)\hat{\omega}(t) \\ &= G(t)\left(\hat{\omega}(t) - (G^\top(t)\omega_d(t))^\wedge\right) \quad (\text{V.7}) \\ &= G(t)(\omega(t) - G^\top(t)\omega_d(t))^\wedge \\ &= G(t)\hat{e}_\omega(t). \end{aligned}$$

Using the trace identity $\text{tr}[A\hat{x}] = -x^\top(A - A^\top)^\vee$ and the definition of $e_{K,R}(t)$ yields

$$\begin{aligned} \dot{\Psi}(t) &= -\frac{1}{2}\text{tr}(K_R G(t)\hat{e}_\omega(t)) \\ &= \frac{1}{2}e_\omega^\top(t)(K_R G(t) - (K_R G(t))^\top)^\vee \quad (\text{V.8}) \\ &= e_\omega^\top(t)e_{K,R}(t). \end{aligned}$$

• **The derivative of $e_{K,R}(t)$:** Let $A(t) = K_R G(t)$, since $K_R \in \mathbb{S}_{++}^3$, $A^\top(t) = G^\top(t)K_R$. Using the identity $M\hat{x} + \hat{x}M^\top = ((\text{tr}(M)I - M)x)^\wedge$, it follows that

$$\begin{aligned} \dot{e}_{K,R}(t) &= \frac{1}{2}(A(t)\hat{e}_\omega(t) + \hat{e}_\omega(t)A^\top(t))^\vee \\ &= \frac{1}{2}(\text{tr}(A(t))I_3 - A(t))e_\omega(t) = \mathcal{C}(t)e_\omega(t). \quad (\text{V.9}) \end{aligned}$$

• **The derivative of $e_\omega(t)$:** Let $G(t) = R_d^\top(t)R(t)$, $e_\omega(t) = \omega(t) - G^\top(t)\omega_d(t)$. Given the definition of $\hat{\omega}(t)$ and $\tau(t)$, then

$$\begin{aligned} \dot{e}_\omega(t) &= \dot{\omega}(t) - \dot{G}^\top(t)\omega_d(t) - G^\top(t)\dot{\omega}_d(t) \\ &= \dot{\omega}(t) - \hat{e}_\omega^\top(t)G^\top(t)\omega_d(t) - G^\top(t)\dot{\omega}_d(t) \\ &= J^{-1}(-\omega(t) \times J\omega(t) + \tau(t)) \\ &\quad + \hat{e}_\omega(t)G^\top(t)\omega_d(t) - G^\top(t)\dot{\omega}_d(t) \quad (\text{V.10}) \\ &= J^{-1}(-e_{K,R}(t) - K_\omega e_\omega(t)) \\ &\quad - \hat{\omega}(t)G^\top(t)\omega_d(t) + \hat{e}_\omega(t)G^\top(t)\omega_d(t) \end{aligned}$$

APPENDIX V. PROOF OF LEMMA 2

The bound on $\|\mathcal{C}(t)\|$ is used in I. We provide a brief proof using our notation, following Proposition 2 in [23]. Let $A(t) := K_R G(t)$. Since $G(t) \in \text{SO}(3)$, it follows that

$$\|\mathcal{C}(t)\|^2 \leq \frac{1}{4}((\text{tr}[A(t)])^2 + \text{tr}[A^\top(t)A(t)]). \quad (\text{V.1})$$

Using the cyclic property of the trace,

$$\text{tr}[A^\top(t)A(t)] = \text{tr}[G^\top(t)K_R^2 G(t)] = \text{tr}[K_R^2]. \quad (\text{V.2})$$

Since $K_R = \text{diag}(k_{R,1}, k_{R,2}, k_{R,3})$ and $|G_{ii}(t)| \leq 1$,

$$|\text{tr}[A(t)]| = |\text{tr}[K_R G(t)]| \leq \sum_{i=1}^3 k_{R,i} = \text{tr}[K_R]. \quad (\text{V.3})$$

Therefore,

$$\|\mathcal{C}(t)\|^2 \leq \frac{1}{4}((\text{tr}[K_R])^2 + \text{tr}[K_R^2]) \leq \frac{1}{2}(\text{tr}[K_R])^2, \quad (\text{V.4})$$

which implies $\|\mathcal{C}(t)\| \leq \frac{1}{\sqrt{2}}\text{tr}[K_R]$.

APPENDIX VI. PROOF OF LEMMA 3

Let $G(t) := R_d^\top(t)R(t) \in \text{SO}(3)$. Then,

$$\begin{aligned} \|(b_{3,d}^\top(t)b_3(t) - b_{3,d}(t))^\wedge\|^2 &= 1 - (b_{3,d}(t) \cdot b_3(t))^2 \\ &= 1 - G_{3,3}^2(t), \quad (\text{VI.1}) \end{aligned}$$

where $G_{3,3}(t)$ denotes the (3, 3) entry of $G(t)$.

Let $x = [x_1, x_2, x_3]^\top \in \mathbb{R}^3$ be the rotation vector such that $G(t) = \exp(\hat{x})$, where $\hat{x} \in \mathfrak{so}(3)$ is the skew-symmetric matrix associated with x , and let the rotation angle be $\|x\| = \theta \in [0, \pi]$. Define the unit rotation axis $u = x/\|x\| = [u_1, u_2, u_3]^\top$. By Rodrigues' formula [35, Lemma 2.3],

$$G(t) = I + \sin \theta \hat{u} + (1 - \cos \theta) \hat{u}^2. \quad (\text{VI.2})$$

Hence, the (3, 3) entry of $G(t)$ is

$$\begin{aligned} G_{3,3}(t) &= \cos \theta + (1 - \cos \theta)u_3^2 \\ &= \cos \theta + (1 - \cos \theta)\frac{x_3^2}{\|x\|^2}. \quad (\text{VI.3}) \end{aligned}$$

Define $T := \frac{(x_1^2 + x_2^2)(\cos \theta - 1)}{\|x\|^2}$. Then, by (VI.3), we have $G_{3,3}(t) = 1 + T$, and therefore

$$\begin{aligned} 1 - G_{3,3}^2(t) &= 1 - (1 + T)^2 \\ &= -2T - T^2 \leq -2T. \quad (\text{VI.4}) \end{aligned}$$

Since $(x_1^2 + x_2^2)/\|x\|^2 \leq 1$ and $1 - \cos \theta \geq 0$, it follows that

$$\begin{aligned} 1 - G_{3,3}^2(t) &\leq -2T \\ &= 2 \frac{(x_1^2 + x_2^2)(1 - \cos \theta)}{\|x\|^2} \quad (\text{VI.5}) \\ &\leq 2(1 - \cos \theta). \end{aligned}$$

From [23], $\Psi_K(t)$ can be expressed as

$$\Psi_K(t) = \frac{1 - \cos(\|x\|)}{2\|x\|^2} \sum_{(i,j,k) \in \mathcal{C}} (k_{R,i} + k_{R,j})x_k^2, \quad (\text{VI.6})$$

where $\mathcal{C} = \{(1, 2, 3), (2, 3, 1), (3, 1, 2)\}$.

Since $h_1 = \min\{k_{R,1} + k_{R,2}, k_{R,2} + k_{R,3}, k_{R,1} + k_{R,3}\}$, we have

$$\sum_{(i,j,k) \in \mathcal{C}} (k_{R,i} + k_{R,j})x_k^2 \geq h_1 \sum_{k=1}^3 x_k^2 = h_1 \|x\|^2. \quad (\text{VI.7})$$

Substituting this into (VI.6) gives

$$\begin{aligned} \Psi_K(t) &\geq \frac{1 - \cos(\|x\|)}{2\|x\|^2} (h_1 \|x\|^2) \\ &= \frac{h_1}{2} (1 - \cos(\|x\|)). \end{aligned} \quad (\text{VI.8})$$

Thus, $1 - \cos(\|x\|) \leq \frac{2}{h_1} \Psi_K(t)$, together with (VI.5) yields

$$\begin{aligned} \|(b_{3,d}^\top(t)b_3(t)) b_3(t) - b_{3,d}(t)\|^2 &= 1 - G_{3,3}^2(t) \\ &\leq 2(1 - \cos(\|x\|)) \leq \frac{4}{h_1} \Psi_K(t). \end{aligned} \quad (\text{VI.9})$$

Using the quadratic bound $\Psi_K(t) \leq g_2 \|e_{K,R}(t)\|^2$, one has

$$\|(b_{3,d}^\top(t)b_3(t)) b_3(t) - b_{3,d}(t)\| \leq \sqrt{\frac{4g_2}{h_1}} \|e_{K,R}(t)\|. \quad (\text{VI.10})$$

Combining this with the definition of $F_d(t)$ in (19) and Assumption 1, the triangle inequality gives

$$\begin{aligned} \|F_d(t)\| &\leq \| -K_p e_p(t) - K_v e_v(t) + m g e_3 + m \ddot{y}_d(t) \| \\ &\leq \|K_p e_p(t) + K_v e_v(t)\| + m \|b_a\|. \end{aligned} \quad (\text{VI.11})$$

Moreover, by the definition of $\mathcal{V}_1(t)$ in (21),

$$\begin{aligned} \|K_p e_p(t) + K_v e_v(t)\| &= \|[K_p \ K_v] z_1(t)\| \\ &\leq \|[K_p \ K_v] M_1^{-1/2}\| \sqrt{\mathcal{V}_1(t)}. \end{aligned} \quad (\text{VI.12})$$

Therefore, $\|\Delta_f(t)\|$ is bounded by

$$\begin{aligned} \|\Delta_f(t)\| &\leq \|F_d(t)\| \|(b_{3,d}^\top(t)b_3(t)) b_3(t) - b_{3,d}(t)\| \\ &\leq (\|[K_p \ K_v] M_1^{-1/2}\| \sqrt{\mathcal{V}_1(t)} + m \|b_a\|) \sqrt{\frac{4g_2}{h_1}} \|e_{K,R}(t)\|. \end{aligned} \quad (\text{VI.13})$$